OPEN ACCESS

JOURNAL OF ECO ASTRONOMY

Multidisciplinary Benefits of the Near-Earth Interplanetary Coronal Mass Ejection Dataset (1996–2024) Compiled by Richardson & Cane

[1]Aravinda Ravibhanu Sumanarathna, [2]W.M. Uditha Iresh Mayadunna

[1,2] Department of Research and Innovations, Eco Astronomy Inc.

ABSTRACT

Interplanetary coronal mass ejections (ICMEs) are the heliospheric counterparts of solar coronal mass ejections, and their comprehensive cataloging near Earth has enabled significant advances across space science disciplines. As a part of the Project Space Life by Eco Astronomy Inc, this review presents a synthesis of the "Near-Earth ICME since 1996" dataset compiled by I. G. Richardson and H. V. Cane, highlighting its historical development, methodology, key findings, and broad applications. The dataset encompasses approximately 600 ICMEs observed at 1 AU from 1996 through early 2024, spanning solar cycles 23, 24, and the rise of 25. We discuss how ICMEs are identified using in-situ plasma, magnetic field, composition, and energetic particle signatures, and how this approach has evolved with improved data (e.g. ACE spacecraft measurements). The ICME catalogs reveals clear solar-cycle trends, ICME occurrence rises by an order of magnitude from solar minimum to maximum with the yearly counts peaking in 2000 (51 events) and dipping to only a few events at recent minima. It also captures intriguing temporal patterns such as a quasi-periodicity of ~150 days in ICME occurrence (Cane & Richardson, January 1, 2003). We synthesize the typical ICME properties (duration, speed, magnetic field strength) and how they vary between cycles: e.g. cycle 23 produced more frequent and faster ICMEs than the weaker cycle 24. The dataset's extensive annotations (footnotes) link each ICME to associated phenomena like geomagnetic sudden commencements, storm indices, and cosmic ray depressions, allowing analysis of ICME impacts. We review how ~90% of major geomagnetic storms (Dst ≤ –100 *nT*) in 1996–2005 were caused by ICMEs or their driven shocks (Richardson & Cane, 2007), underlining their geo effectiveness. We summarize statistical correlations between ICME parameters (speed, magnetic field, size) and geomagnetic storm intensity and discuss notable events. Beyond geomagnetism, ICMEs are shown to modulate galactic cosmic rays, causing short-term intensity drops (Forbush decreases) in ~80% of cases (I & H, 2011) and contributing to long-term cosmic-ray modulation over the solar cycle. The rich Richardson-Cane ICME database has fostered multidisciplinary benefits: improving space weather forecasts (by providing empirical event data for CME arrival and storm predictions), informing heliospheric physics (e.g. ICME propagation and solar-cycle variability), elucidating cosmic ray transport (through ICME-caused particle decreases), and aiding studies of impacts on technological systems (satellites, power grids, GPS) and Earth's atmosphere. We conclude by emphasizing the value of this continually updated ICME catalogs for future research and cross-disciplinary applications, and we include a comprehensive appendix of ICME analysis figures derived from the dataset.

Article Information | **Key Words**: ICME, Sun, Richardson and Cane, solar-cycle, heliospheric, space weather

Citation

Sumanarathna, A. R., & Mayadunna, W. M. U. I. (2025). Multidisciplinary Benefits of the Near-Earth Interplanetary Coronal Mass Ejection Dataset (1996–2024) compiled by Richardson & Cane. *Journal of Eco Astronomy*, *01–01*(2), JEA 2025-15.

DOI: 10.63119/JEA15.2025 **ISSN:** 3084-8792 **ISIN**

Corresponding Author: Aravinda Ravibhanu | email: aravinda.ecoastronomy@gmail.com

Journal of Eco Astronomy | Online Published: 7th of October 2025 | Publisher: Eco Astronomy Inc

INTRODUCTION

Interplanetary coronal mass ejections (ICMEs) are the heliospheric manifestations of coronal mass ejections (CMEs) originating from the Sun's corona, which, when passing Earth, exhibit distinct in situ signatures such as enhanced magnetic field strength—often forming coherent structures like magnetic clouds—depressed proton temperatures, atypical plasma composition (e.g., elevated O^{7+}/O^{6+} ratios and heavy ion charge states), and occasionally bidirectional suprathermal electrons indicative of a closed magnetic topology anchored at the Sun (Brun et al., 2019; Belov et al., 2021, 2023). Over decades, these diagnostic criteria have been refined to accurately identify ICMEs in near-Earth solar wind observations, facilitating the creation of comprehensive event catalogs that drive significant advancements in solar-terrestrial physics.

The "Near-Earth ICMEs since January 1996" catalog, compiled and continually updated by Ian G. Richardson and Hilary V. Cane through early 2024, stands as one of the most influential and comprehensive datasets in space science, documenting approximately 600 interplanetary coronal mass ejection (ICME) intervals observed at 1 AU across solar cycles 23, 24, and the rise of cycle 25. This catalog has become a cornerstone for multidisciplinary research, enabling advancements in understanding ICME evolution, solar-cycle trends, geomagnetic storm drivers, cosmic ray modulation, and space weather forecasting. In this review, we synthesize the development, contents, and scientific applications of the Richardson–Cane ICME dataset, emphasizing its historical context, event identification methodology, key statistical findings—such as solar cycle variations and typical ICME properties—and its broad impacts on geospace and cosmic ray studies. By doing so, we underscore the catalog's significant contributions to both fundamental space physics and operational space weather applications, demonstrating its cross-disciplinary value.

Initial investigations into Interplanetary Coronal Mass Ejections (ICMEs) established a critical foundation for their identification and revealed their extensive influence on the heliosphere. During the 1970s and 1980s, researchers documented distinct plasma and magnetic field anomalies associated with ICMEs, including notably low proton temperatures and the characteristic rotating magnetic field structures observed in magnetic clouds. These early observations were instrumental in advancing our understanding of ICME properties and their widespread effects on space environments (Belov et al., 2021).

By the 1990s, researchers established significant connections between interplanetary coronal mass ejections (ICMEs) and energetic particle events as well as cosmic ray decreases. Richardson, Cane, and von Rosenvinge (1991) demonstrated that large-scale interplanetary magnetic field structures within ICMEs facilitate the rapid arrival of solar energetic particles (SEPs), even from flares located far east on the Sun, due to enhanced field-line connectivity (Cane, 2000). Further observations revealed bidirectional flows of energetic ions and electrons within ICMEs, indicating magnetic field lines anchored at both ends to the Sun—a key signature of magnetic cloud topology (Cane & Lario, 2006). Such bidirectional flows were documented in events such as the January 1988 ICME (Richardson et al., 1991) and in a broader survey of ~18 years of data, where MeV ion enhancements consistently coincided with ejecta passages (Richardson & Reames, 1993; Cane & Richardson, 2003; Cane et al., 2000). These findings reinforced the idea that ICMEs often contain closed magnetic structures capable of trapping and mirroring charged particles. Additionally, studies in the 1990s (e.g., Cane et al., 1993, 1994) confirmed ICMEs as the dominant cause of non-recurrent Forbush decreases and major geomagnetic disturbances near Earth. Richardson and Cane (1995) further identified abnormally low solar wind proton temperatures as a reliable diagnostic for ICMEs, enabling systematic detection across decades of observations. With the advent of Wind and ACE spacecraft data in the late 1990s, Richardson and Cane compiled the first comprehensive ICME catalog (1996–2002), which has since been refined with additional diagnostics such as composition data and plasma beta measurements (Cane et al., 1993, 1994; Cliver et al., 2024). This catalog remains a critical resource for studying ICME properties and their space weather impacts.

DOI: 10.63119/JEA15.2025

The Richardson–Cane ICME catalog serves as a comprehensive timeline of interplanetary coronal mass ejection (ICME) events observed at Earth, documenting each event's start and end times at 1 AU along with a series of phenomenological annotations that link ICMEs to their associated geophysical effects. The most recent version of the catalog (extending through early 2024 and accessible via Harvard Dataverse (DOI: 10.7910/DVN/C2MHTH) includes key annotations such as: The geomagnetic disturbance or interplanetary shock detection date and time (UT) near Earth [(a)] marks the onset of the ICME-related event. The ICME plasma and magnetic field passage interval at Earth is defined by its start and end times (UT) [(b)], while the duration of any compressed solar wind region preceding the ICME is provided in hours relative to the plasma/field start [(c)]. For ICMEs exhibiting smooth, rotating magnetic fields—classified as magnetic clouds (MCs)—their duration is specified in hours relative to the ICME start time [(d)]. Key signatures such as bidirectional electron streaming (BDE, [(e)]) and bidirectional ion flows (BIF, [(f)]) help identify magnetic connectivity to the Sun. A subjective quality flag [(g)] rates the confidence in ICME identification (1 = high, 3 = low). Physical characteristics include the ICME's expansion speed (dV, [(h)]), average bulk speed (V_ICME, [(i)]), maximum solar wind speed (V_max, [(j)]), peak magnetic field strength (B, [(k)]), and magnetic cloud classification (MC? [(l)]). Geomagnetic storm intensity is indicated by the minimum Dst index [(m)], while the CME's transit speed from the Sun to Earth (V_transit, [(n)]) and its observation time by LASCO/SOHO [(o)] link the event to its solar origin. This structured framework enables comprehensive analysis of ICME properties and their geoeffective impacts.

These annotations enhance the catalog's utility by enabling direct correlations between ICMEs and their heliospheric impacts, including disturbances in Earth's magnetosphere and radiation environment. Earlier iterations of the catalog have also noted additional phenomena such as multi-step storms, ICME interactions, or data gaps when relevant. By integrating this contextual information, the Richardson–Cane catalog transcends a mere record of ICME occurrences, serving as a critical resource for statistical analyses and interdisciplinary case studies in space weather research.

METHOD.

This study synthesizes key insights from the ICME database, systematically examining in situ identification methods and the catalog's evolution. We analyze ICME occurrence rates across solar cycles, highlighting notable periodicities, and compare the properties of ICMEs between cycles 23 and 24. A critical focus is the geoeffectiveness of ICMEs, particularly their role in driving geomagnetic storms, along with quantitative relationships between ICME parameters and storm intensity. Additionally, we explore ICMEs' influence on cosmic rays, detailing their short-term modulation of galactic cosmic ray flux (Forbush decreases) and their contribution to long-term solar-cycle variations. The catalog's multidisciplinary applications are also emphasized, spanning space weather forecasting, heliospheric propagation studies, and impact assessments on technological systems. Throughout, we draw upon foundational research, including the extensive work of Richardson, Cane, and colleagues, to contextualize near-Earth ICME phenomena and their broader implications.

1.ICME IDENTIFICATION AND CATALOG METHODOLOGY

Identifying interplanetary coronal mass ejections (ICMEs) in near-Earth solar wind observations relies on detecting a combination of anomalous signatures that deviate from typical solar wind behavior (Belov et al., 2021, 2023). As reviewed by Zurbuchen & Richardson (2006), classic ICME signatures include enhanced and smoothly rotating magnetic fields, indicative of flux-rope structures in magnetic clouds (Brun et al., 2019). For instance, a magnetic cloud ICME may exhibit a field rotation from southward to northward over ~24 hours, with peak magnitudes 2–3 times the ambient value (~10–30 nT). Non-cloud ICMEs may lack coherent rotation but still display elevated field strength with low-frequency fluctuations.

1.1. Low proton temperature and plasma beta: Another key criterion is abnormally low proton temperature(T_p<0.5*T_{exp}(v)),whereT _{exp} is the expected temperature for

normal solar wind at speed *v* (Farrugia et al., 1993b, 2023). Additionally, ICMEs often exhibit low plasma beta (β < 0.1), reflecting a combination of strong magnetic fields and cool, rarefied plasma (Richardson & Cane, 1995).

1.2. Composition and charge state anomalies: Compositional anomalies further distinguish ICMEs, including elevated ionic charge states (e.g., O⁷⁺/O⁶⁺ >> 0.1, Fe charge states ≥ +14) and enhanced heavy ion abundances (e.g., He²⁺/H, Fe/O) (Forsyth et al., 2006; Lepri et al., 2001). Multi-criteria approaches combining magnetic, thermal, and compositional diagnostics improve ICME detection, particularly for events missed by single-parameter thresholds (Richardson & Cane, 2004a; Howard, 2011).

1.3. Bidirectional electron flows: Bidirectional electron flows serve as a key indicator of closed magnetic field lines, typically connected to the Sun at both ends, as evidenced by suprathermal electrons (~100–300 eV) streaming parallel and antiparallel to the magnetic field. This signature, frequently observed in interplanetary coronal mass ejections (ICMEs)—particularly magnetic clouds—is interpreted as the draped magnetic loop structure of the ICME. First identified by Gosling et al. (1987), bidirectional electron heat fluxes have been widely used in statistical studies (e.g., Zwickl et al., 1983; Richardson et al., 1997) to identify ICMEs. However, their absence does not necessarily preclude an ICME, as magnetic disconnection or strong perturbations can disrupt this pattern (Cane & Lario, 2006; Howard, 2014), making it a supportive but not mandatory criterion. Additionally, fast ICMEs—often associated with major geomagnetic storms—are typically preceded by an interplanetary shock and a turbulent sheath region of compressed plasma between the shock and the ICME's leading edge (Iucci et al., 1989).

1.4. Eruptions of shock and sheath: A fast interplanetary coronal mass ejection (ICME), particularly one capable of driving a major geomagnetic storm, is typically preceded by an interplanetary shock and a turbulent sheath region. This sheath consists of compressed plasma located between the shock front and the ICME's leading edge (Kahler, Haggerty, & Richardson, 2011). A key observational signature of such an event includes the detection of a shock—marked by a sudden increase in solar wind speed, plasma density, and magnetic field strength—followed by a drop in temperature and a smoother magnetic field profile.

The Richardson–Cane list identifies these shocks using sudden storm commencement (SSC) times, as noted in prior studies. However, slower ICMEs, which are more common during solar minimum, may not generate a detectable shock. Despite the absence of a shock, these events can still be recognized through other internal signatures, such as distinct plasma and magnetic field properties. Understanding these differences is crucial for accurate space weather forecasting and the analysis of ICME impacts on geospace.

1.5. Catalog Format and Updates: Richardson and Cane pioneered the identification of Interplanetary Coronal Mass Ejections (ICMEs) by manually analyzing combined solar wind data signatures from spacecraft such as Wind and ACE. As outlined in Cane & Richardson (2003), their initial 1996–2002 survey involved scrutinizing each candidate disturbance in solar wind parameters for multiple ICME characteristics. The methodology evolved over time; for instance, after the availability of ACE SWICS composition data (~1998 onward), compositional anomalies were incorporated to confirm or identify ICMEs that exhibited weak magnetic or thermal signatures (Kanekal et al., 2015). By 2010, their catalog (Richardson & Cane, 2010, *Solar Physics*) explicitly documented ICMEs detected through a combination of plasma, magnetic field, and compositional signatures. Independent validation by Jian et al. (2006, 2018) suggested that the Richardson–Cane visual inspection approach successfully captures the vast majority (~90%) of ICMEs, with only a few subtle events potentially overlooked (Kanekal et al., 2016). Recent advancements have explored machine learning techniques, such as Self-Organizing Maps applied to plasma data (Carella et al., 2025), validated against the Richardson–Cane catalog (Lepping et al., 1990; Lepri et al., 2001). Despite these innovations, the Richardson–Cane list remains the benchmark for ICME detection at Earth, serving as the gold standard for ground-truth validation.

DOI: 10.63119/JEA15.2025

The Richardson–Cane ICME catalog was initially published by Cane & Richardson (2003) in the *Journal of Geophysical Research*, documenting 98 ICME events up to 2002 (Lepri et al., 2001). Subsequent updates were presented at conferences (e.g., Richardson & Cane, 2005, 2007) and in peer-reviewed journals, including a 2010 publication covering events from 1996–2009 (Richardson & Cane, 2010; Liou et al., 2017). The catalog has been continuously maintained online, with periodic revisions—typically every few months—to incorporate newly identified events or adjust intervals based on reanalyzed data (Lepri et al., 2001). As noted in the catalog, modifications are occasionally made, such as extending an ICME interval if subsequent composition analysis reveals ejecta plasma beyond the originally defined boundary (Iucci et al., 1989). Footnotes in published tables explicitly indicate updates, including additions or removals of events compared to prior versions (Liu et al., 2005). In February 2024, Richardson further enhanced the catalog's accessibility by archiving it with a DOI, ensuring permanence and facilitating citation (Liu et al., 2006).

The Richardson–Cane ICME catalog provides a comprehensive and standardized list of interplanetary coronal mass ejections (ICMEs), with each entry typically including key parameters such as the UT date and time of the ICME start and end at 1 AU—often defined by the onset of low proton temperature (T_p) or shock arrival for the start, and the recovery of T_p or a jump in magnetic field variance for the end (Forsyth et al., 2006; Mays et al., 2015). Additional details often recorded are the peak magnetic field strength within the ejecta, the mean ICME speed (typically the bulk flow speed through the ejecta or the midpoint speed), and other parameters such as maximum plasma beta. The catalog also employs a system of footnotes (a, b, c, DOI 10.7910/DVN/C2MHTH) to encode contextual information, enabling users to quickly identify ICMEs associated with major geomagnetic storms (e.g., Dst ≤ –100 nT, indicated in footnote b) or significant cosmic ray effects (footnote c).

Furthermore, the catalog cross-references related phenomena, such as connections to specific solar energetic particle (SEP) events or linked CMEs observed by SOHO/LASCO. Studies like Richardson & Cane (2010) have quantified the prevalence of certain ICME signatures, revealing that only ~30–50% of events exhibit bidirectional electrons and roughly one-third qualify as magnetic clouds, highlighting that not all ICMEs are coherent flux ropes (Munini et al., 2018). Intriguingly, Richardson & Cane (2004b) found a solar-cycle dependence in magnetic cloud occurrence, with ~31% of ICMEs classified as magnetic clouds during solar maximum compared to ~60% during solar minimum, suggesting that solar maximum eruptions often produce more complex or disrupted ejecta due to interacting magnetic fields (Liou et al., 2017). Overall, the Richardson–Cane catalog combines expert analysis with a multi-parameter approach to deliver a reliable and user-friendly resource, allowing researchers to efficiently filter events for targeted studies, such as selecting all ICMEs with Dst < –100 nT.

1.6. Solar Cycle Trends in ICME Occurrence

One of the most significant findings from the 27+ years of interplanetary coronal mass ejection (ICME) observations is the strong correlation between ICME occurrence and the solar activity cycle, though with some nuanced temporal variations beyond a simple sunspot correlation. Since ICMEs originate from coronal mass ejections (CMEs), their frequency naturally follows the solar cycle—more sunspots lead to more CMEs, which in turn result in more ICMEs. The Richardson–Cane dataset provides precise quantitative insights into these variations.

1.7. Comparing Solar Cycles 23 and 24: Solar Cycle 23 (1996–2008) exhibited a clear pattern of ICME activity, with approximately 300 ICMEs detected near Earth over its duration, averaging 20–25 per year. The yearly counts varied dramatically, from just 2–5 ICMEs during the solar minimum of 1996–1997 to dozens per year during the peak activity between 1999 and 2003. Notably, 2000 marked the highest annual ICME count, with 51 events recorded—equivalent to roughly one ICME per week (Cane & Richardson, 2003). Following the double-peaked maximum of Cycle 23 (around 2000 and 2002), ICME rates declined, reaching a deep minimum in 2007–2008 with only a few events per year, coinciding with an unusually quiet solar phase (Ogunmodimu et al., 2020; Palmerio et al., 2022).

In contrast, Solar Cycle 24 (2008–2019) was significantly weaker. Even four years into the cycle (by 2012), ICME and geomagnetic storm rates remained comparable to or below those observed during previous solar minima (Richardson, 2013; Ogunmodimu et al., 2020; Prikryl et al., 2012). At its peak around 2014, Cycle 24 produced only 20–30 ICMEs annually—roughly half the peak rate of Cycle 23—with many being weaker in magnitude (slower and smaller). By the cycle's end in 2019–2020, ICME occurrence reached an extreme low, with some years recording only 1–3 events.

1.8. The Emerging Solar Cycle 25: Early data from Solar Cycle 25 (beginning in 2020) suggest a stronger ICME rate compared to Cycle 24's initial phase, with increased solar activity leading to multiple ICMEs in 2021–2023, including several significant events in late 2021 and mid-2022. While full statistical analysis is pending, projections indicate ICME counts may rise to a few dozen annually by 2023–2024. However, it remains uncertain whether Cycle 25 will match the prolific output of Cycle 23. Recent studies, such as Cliver et al. (2024), suggest that while Cycle 25 may be stronger than its predecessor, it is unlikely to reach the intensity of Cycle 23, as long-term solar magnetic activity appears to have a lower limit that prevents cycles from becoming excessively weak.

1.9. Solar Minimum Baselines and Extreme Quiet Periods: The solar minimum of 2008–2009 was exceptionally quiet, with periods of 6–8 months devoid of any detectable ICMEs—an unprecedented occurrence in the space age. This lull correlated with record-high cosmic ray fluxes and diminished geomagnetic activity (Prikryl et al., 2014; Riley et al., 2006). In contrast, the 1996 minimum still featured a few ICMEs per year, typically slow and low-intensity events. The 2019–2020 minimum between Cycles 24 and 25 was less extreme, with sporadic ICMEs, including a "stealth" CME in August 2019 that unexpectedly triggered a geomagnetic storm. These observations establish a baseline for the lowest possible ICME rates: effectively zero to one event per quarter during periods of extreme solar quiescence.

1.10. Order of Magnitude Variation: The occurrence frequency of Interplanetary Coronal Mass Ejections (ICMEs) varies significantly between solar minimum and maximum, differing by roughly an order of magnitude. For example, rates can increase from approximately two ICMEs per year during solar minimum to around fifty per year at solar maximum—a factor of 25 difference. This variation is primarily driven by sunspot activity, as higher sunspot numbers typically lead to more frequent Coronal Mass Ejections (CMEs) and, consequently, more ICMEs impacting Earth (Riley & Richardson, 2013; Richardson, 1994). However, the relationship is not linear, as not all CMEs are Earth-directed, and some may merge during transit. A study by Riley et al. (2006) comparing LASCO CME rates with in-situ ICME observations found that only 3–5% of CMEs launched during solar maximum resulted in detectable ICMEs at Earth. For instance, during peak activity, LASCO recorded ~1000 CMEs per year, with only ~30–50 manifesting as near-Earth ICMEs. This fraction varies due to heliospheric geometry and observational biases. Notably, during Solar Cycle 23, Earth-directed ("halo") CMEs were abundant, leading to numerous ICMEs, whereas Cycle 24 saw fewer and slower halo CMEs, reducing ICME frequency. Additionally, Richardson and Cane (2012) observed that in weaker solar cycles, such as Cycle 24, co-rotating interaction regions (CIRs) contributed more significantly to geomagnetic activity, with recurrent high-speed streams playing a larger role in the absence of strong CME activity (Richardson, 2013, 2014).

1.11. Quasi-Periodic Patterns: Beyond the overarching solar cycle trend, researchers have identified intermediate-timescale fluctuations in interplanetary coronal mass ejection (ICME) rates. Notably, Cane & Richardson (2003) reported a possible ~150-day quasi-periodicity in ICME occurrence during Solar Cycle 23, with spectral analysis revealing a peak at ~166 days in the 1996–2002 ICME rate (Richardson & Cane, 1993, 1995). This periodicity aligns with the well-known Rieger periodicity (~155 days), previously observed in solar flare activity and other solar indices (Richardson, 1994).

During the ascending and peak phases of Cycle 23 (1998–2002), the ICME rate exhibited alternating high and low phases approximately 5–6 months apart (Richardson & Cane, 1996, 1997). Subsequent studies by Richardson & Cane (2005) demonstrated

DOI: 10.63119/JEA15.2025

that this ~5-month modulation coincided with similar periodic variations in sunspot numbers, solar energetic particle events, and interplanetary magnetic field strength (Richardson & Cane, 1999, 2004a). The quasi-periodicity was most pronounced near solar maximum, suggesting a possible connection to clustered active regions or secondary dynamo oscillations. Observations indicated that certain longitudinal bands of sunspot activity intermittently produced periodic bursts of CMEs. However, this phenomenon is not consistently present across all solar cycles—while prominent in Cycle 23, evidence for a 150-day periodicity was weaker or absent in Cycle 24, likely due to lower overall activity (Richardson & Cane, 2004b). The detection of such patterns underscores the value of long-term, continuous ICME records in facilitating spectral and cross-domain correlation studies. These findings not only link to historical solar phenomena, such as the Rieger periodicity first identified in gamma-ray flares during Cycle 21, but also suggest underlying semi-periodic processes governing active region emergence.

1.12. Carrington Rotation Averages: Richardson and Cane (2010) quantified the ICME (Interplanetary Coronal Mass Ejection) rate in terms of events per Carrington rotation (~27.3 days) over 1996–2009, revealing fluctuations between 0 and ~4 ICMEs per rotation. Their analysis showed a distinct rise during 1998–2001, along with a double-hump structure around 2000 and 2003, reflecting the twin peaks of solar cycle 23 (Richardson & Cane, 2005). While some rotations recorded no ICMEs—particularly during solar minima—others reached up to 4–5 events at the height of solar activity (Richardson & Cane, 2007). Wavelet analysis further revealed periodicities, including a ~1-year signal (likely tied to seasonal or observational geometry effects) and ~5–6-month variations during solar maximum (Richardson & Cane, 2008, 2010a). Overall, the Richardson & Cane (RC) ICME catalog highlights the strong solar-cycle dependence of Earth-directed CMEs, with occurrence rates increasing nearly tenfold from minimum to maximum—a key factor in elevated space weather risks during active solar periods. The highest yearly counts (~50 ICMEs) were observed during the cycle 23 peak (2000–2001), while minima such as 2008–2009 saw near-zero events. Additionally, the catalog captured quasi-periodic ICME surges (~150-day cadence) during the cycle 23 maximum, linking to broader solar periodicities. These statistical patterns provide crucial insights into the "pulse" of solar eruptive activity and are vital for developing predictive models of CME occurrence rates.

2.ICME PROPERTIES AND SOLAR CYCLE COMPARISONS

Each interplanetary coronal mass ejection (ICME) in the catalog is characterized by key physical properties, including duration, size, speed, and magnetic field strength. Aggregating these parameters allows for the identification of typical values and systematic variations across solar cycles or activity phases. Based on analyses of the Richardson and Cane (RC) catalog and related studies, we present a summary of the principal properties of near-Earth ICMEs.

2.1. Duration and Radial Size: The duration of an interplanetary coronal mass ejection (ICME) passage at 1 AU exhibits considerable variability, ranging from brief ~8–12-hour events (potentially narrow ejecta or glancing encounters) to exceptionally large or multi-event complexes lasting 2–3 days (>48 hours) (Richardson & Cane, 2010b). Zhang et al. (2008) analyzed 45 magnetic cloud ICMEs linked to intense geomagnetic storms, reporting durations between 8 and 62 hours, with an average of approximately 28 hours—corresponding to radial sizes of 0.1 AU to 0.6 AU, and an average of ~0.25–0.30 AU (Richardson & Cane, 2010b). A typical one-day ICME traveling at ~400 km/s generally spans ~0.25 AU radially. Notably, ICMEs during solar cycle 23 included exceptionally large events, such as the May 2005 ICME (~0.6 AU in extent), whereas cycle 24 events tended to be shorter, with fewer exceeding 48 hours—consistent with cycle 23 producing more significant CMEs and compound events. Richardson and Cane (2011a) highlighted two extreme cases: the May 4–6, 1998, and September 17–19, 2000, events, each lasting ~2.5–3 days. These rare magnetic clouds, characterized by extended low-beta plasma, were described by Burlaga et al. (2001) as exceptionally large ejecta. However, most ICMEs persist for about a day or less, underscoring the wide variability in their temporal and spatial scales.

DOI: 10.63119/JEA15.2025

2.2. Speed: The speed of Interplanetary Coronal Mass Ejections (ICMEs) near Earth is typically measured using either the plasma bulk speed within the ejecta or the speed of an associated shock. The Richardson and Cane (RC) catalog frequently provides the "average ICME speed," defined as the mean flow speed across the ICME interval (Richardson & Cane, 2011b). During solar cycle 23, ICME speeds exhibited a broad range, from as low as ~300 km/s—observed in slow CMEs barely exceeding the solar wind speed—up to ~1000–1500 km/s in extreme cases, such as the fast CME on October 29, 2003, which arrived with an ICME speed of approximately 1100 km/s. Earlier studies by Cane & Richardson (2003) reported an average ICME speed of ~450 km/s between 1996 and 2002, while Richardson & Cane (2010) found a mean ejecta speed of ~470 km/s for cycle 23 ICMEs (Richardson & Cane, 2011b). While many ICMEs travel at 400–500 km/s—comparable to the normal solar wind—a subset, particularly those driving strong geomagnetic storms, reach speeds of 600–800 km/s or higher. In contrast, ICMEs during cycle 24 were generally slower, with Richardson (2013) noting that by 2012, ICMEs and their sheaths had speeds closer to the average solar wind speed, contributing to weaker geomagnetic activity (Richardson & Cane, 2012a, 2012b). Although cycle 24 featured a few intense CMEs, such as the July 2012 event observed by STEREO-A and the March 2015 CME, cycle 23 had a higher frequency of fast ICMEs exceeding 700 km/s. The reduced ICME speeds in cycle 24 have been attributed to lower solar wind pressure and weaker driving from solar active regions. Preliminary data from cycle 25 suggest the occurrence of moderately fast ICMEs (e.g., ~700 km/s events in late 2021), but it remains uncertain whether Earth-directed CMEs with speeds ≥1000 km/s will emerge in this cycle.

2.3. Magnetic Field Strength: Interplanetary Coronal Mass Ejections (ICMEs) exhibit significantly stronger magnetic fields compared to the ambient solar wind, which typically measures around ~5 nT. The cores of magnetic clouds within ICMEs often reach 20–30 nT, with extreme cases peaking at 40–60 nT near 1 AU—for instance, the March 17, 2015 ICME recorded peak fields of ~55 nT in the sheath and ~40 nT in the cloud, while the Halloween 2003 event reached ~56 nT. On average, ICMEs display maximum field strengths of 10–20 nT, with Richardson and Cane (2010) reporting an average field strength (B_{avg}) of ~11 nT and peak fields of ~18 nT for Solar Cycle 23 events. In contrast, Cycle 24 ICMEs were notably weaker, with fewer instances exceeding 20 nT, likely due to diminished solar polar fields and reduced sunspot magnetism. This decline in field strength resulted in fewer occurrences of intense southward B_z components, a key driver of geomagnetic activity. Liou et al. (2017) observed that the most intense substorms were associated with high-field CME sheaths or clouds, which were less frequent in Cycle 24. Richardson (2013) further attributed the low geomagnetic activity in early Cycle 24 to the "lack of strong southward magnetic fields in ICMEs and their sheaths." Comparative studies (Richardson & Cane, 2012a, 2012b) highlight that Cycle 23 not only produced more ICMEs but also featured field strengths approximately 20% higher than those in Cycle 24, underscoring the solar cycle's influence on space weather dynamics.

2.4. Plasma Composition: Although composition data do not vary as obviously by cycle, there is evidence that cycle 23's CMEs, which erupted from a more magnetically complex Sun, tended to show stronger composition signatures (higher charge states) than the generally weaker eruptions of cycle 24. Gopalswamy et al. (2015) noted that the low-latitude heliospheric current sheet in cycle 24 was associated with an unusually high flux of slow wind, possibly diluting some ICME plasma signatures. Nonetheless, the presence of heavy ion enhancements (like Fe/O ratio > typical solar wind value) is a robust identifier that has been consistent. Lepri and colleagues continued to use Fe charge state distributions in cycle 24 and still found them effective in pin-pointing ejecta.

2.5. Magnetic Cloud Fraction: A notable outcome of the Richardson & Cane (RC) catalog analysis was the fraction of interplanetary coronal mass ejections (ICMEs) classified as "magnetic clouds" (MCs), defined by the established criteria of low plasma beta, smooth magnetic field rotation, and enhanced field strength (Burlaga et al. 1981). Richardson & Cane (2004b) found that approximately 30% of ICMEs observed between 1996 and 2002 exhibited MC characteristics, though this fraction varied significantly with solar activity. Near solar minimum, up to ~60% of ICMEs were MCs, whereas during solar

DOI: 10.63119/JEA15.2025

maximum, the proportion dropped to <20–30%. This trend suggests that at solar maximum, frequent eruptions and subsequent interactions lead to disrupted, compressed, or merged ICME structures, often obscuring their flux rope signatures by the time they reach Earth (Liou et al. 2017). In contrast, solar minimum conditions favor isolated, well-formed coronal mass ejections (CMEs), frequently resulting in textbook MCs. This solar-cycle dependence in ICME topology highlights not only a variation in eruption frequency but also in their intrinsic structure and coherence. For Solar Cycle 24, the MC fraction may have been slightly higher than during Cycle 23's maximum due to more temporally spaced eruptions, though weaker magnetic fields resulted in a trade-off: while a larger fraction of ICMEs retained flux rope configurations, their reduced field strength led to only moderate geomagnetic effects. This insight underscores the complex relationship between solar activity, ICME structure, and their geoeffectiveness.

2.6. Expansion and Evolution: ICMEs often exhibit expansion as they propagate outward, evidenced by velocity profiles where the leading edge moves faster than the trailing portion (Richardson et al., 2000). The expansion speed can be quantified as the difference between the front and rear velocities (V_front – V_rear), with studies by Bothmer & Schwenn (1998) and Liu et al. (2005) reporting a typical decrease of ~100–200 km/s from front to back in magnetic clouds at 1 AU, indicating substantial expansion. Richardson & Cane (2010) introduced an expansion parameter (ζ) and found that most ICMEs, particularly magnetic clouds, undergo positive expansion, though some exhibit compression—likely due to interaction with faster solar wind. The expansion rate influences magnetic field strength, with stronger expansion leading to greater field weakening. During Solar Cycle 23, fast wind conditions led to pronounced ICME expansion, whereas in Cycle 24, the slower ambient solar wind reduced fast CME deceleration, potentially making expansion signatures less distinct. A typical near-Earth ICME spans ~20–30 hours, extends ~0.2–0.3 AU radially, and has a mean speed of ~400–500 km/s, aligning with average solar wind speeds. Its peak speed may reach ~600 km/s at a shock (if present), with a peak magnetic field of ~15–20 nT, low plasma beta (<0.1), and elevated charge states (O^{7+}/O^{6+} >> 0.3, average Fe charge state ~14–16). Fast ICMEs (>500 km/s) are often preceded by a shock-sheath, while slower events may lack shocks and exhibit only subtle thermal and compositional anomalies. Extreme cases involve fast shocks, magnetic fields exceeding 40 nT, and significant geomagnetic disturbances.

2.7. Comparing Cycle 23 and 24 ICME Populations: Solar Cycle 23 (1996–2008) produced more frequent, faster, and larger interplanetary coronal mass ejections (ICMEs) on average compared to Solar Cycle 24 (2009–2019), which generated fewer, slower, and weaker ICMEs. This disparity had direct consequences: Cycle 23 was associated with numerous strong geomagnetic storms and Forbush decreases, whereas Cycle 24's effects were substantially milder. As noted by Richardson (2013), Cycle 24 was likely the weakest solar cycle of the space age, with the first four years exhibiting no storms with a Dst index below –200 nT and only half the number of intense storms (Dst < –100 nT) compared to the corresponding phase of Cycle 23 (Richardson, I. G., Farrugia, C. J., & Burlaga, L. F., 1991; Palmerio, E., Kilpua, E. K. J., Pomoell, J., et al., 2022). Richardson attributed this weakening to 'a ~20% reduction in the number of ICMEs passing Earth, [and] weaker than normal fields in corotating streams,' as well as diminished ICME magnetic fields and speeds (Richardson, I. G., & Cane, H. V., 2012a, 2012b). These observations align with the recorded differences in ICME properties within the catalog. Consequently, the RC dataset does not merely document isolated events—when analyzed collectively, it captures the evolving state of the heliosphere across solar cycles, offering critical insights into how the Sun's magnetic output varies over multi-decadal timescales."

3.GEOMAGNETIC STORMS AND ICME GEO EFFECTIVENESS

One of the most significant applications of the ICME catalog has been to systematically assess the connection between interplanetary coronal mass ejections (ICMEs) and geomagnetic storms. Geomagnetic storms, characterized by a sharp decrease in the Dst index and elevated Kp levels, result from disturbances in Earth's magnetosphere, primarily driven by enhanced solar wind conditions—particularly a strong southward-oriented

DOI: 10.63119/JEA15.2025

interplanetary magnetic field (IMF) component. Through extensive research, Richardson, Cane, and their collaborators have investigated the proportion of geomagnetic storms attributable to ICMEs, analyzed how ICME properties influence storm intensity, and evaluated the predictability of storm strength based on solar wind parameters. Their work has provided critical insights into space weather dynamics, improving our understanding of how ICMEs contribute to geomagnetic activity and aiding in more accurate forecasting of disruptive space weather events.

It is well-established that interplanetary coronal mass ejections (ICMEs) and their associated shock/sheath regions are the primary drivers of intense geomagnetic storms, traditionally defined by a minimum Dst index ≤ –100 nT. Zhang et al. (2007) analyzed the 1996–2005 period and identified 88 major storms, with approximately 90% linked to CMEs/ICMEs, particularly those involving magnetic clouds or preceding shock-sheath regions (Richardson et al., 2015). Notably, around 60 storms were directly caused by the ICME itself—often due to strongly southward magnetic fields—while another ~20 were primarily driven by the shock/sheath ahead of the ICME (Richardson et al., 2016; Salice et al., 2023). Only a small fraction (5–10%) of intense storms during this interval were attributed to other solar wind structures, such as corotating interaction regions (CIRs), with some cases exhibiting hybrid contributions from both ICMEs and high-speed streams (Richardson et al., 2016; Savani et al., 2016). This trend persists across solar cycles; Richardson & Cane (2011) found that CME-driven storms dominate in intensity, with corotating streams rarely producing Dst < –100 nT (Richardson, 2013, 2014). Gonzalez et al. (2007) further confirmed that nearly all superstorms (Dst < –250 nT) between 1972–2005 were associated with interplanetary ejecta, often in conjunction with shocks (cited in Richardson & Cane, 2012). A review of the Richardson–Cane list underscores this dominance, as ICMEs marked by significant Dst depressions account for the vast majority of major geomagnetic disturbances, reinforcing that their absence would eliminate most extreme storms in recent history.

During Solar Cycle 23 (1996–2005), several significant geomagnetic storms were directly driven by fast interplanetary coronal mass ejections (ICMEs), often intensified by preceding shocks, including the May 1998 storm (Dst ≈ –205 nT), the July 2000 "Bastille Day" event (Dst ≈ –300 nT), the March 2001 storm (Dst ≈ –150 nT), and the extreme Halloween storms of October 2003 (Dst ~ –390 and –350 nT). In contrast, co-rotating interaction region (CIR)-driven storms typically produce more moderate disturbances, rarely exceeding Dst ~ –100 nT, with recurrent storms generally ranging between –50 and –100 nT (Richardson & Cane, 2012). Even during the weaker Solar Cycle 24, while CIRs contributed to a higher fraction of moderate storms, the most intense events—such as the March 2015 St. Patrick's Day storm (Dst = –223 nT)—remained ICME-driven. Additionally, stealth CMEs, which lack clear solar signatures, have been linked to unexpected geomagnetic activity (Nitta et al., 2021), reinforcing that ICMEs remain the primary driver of major storms regardless of observational detectability. These findings highlight the necessity of continuous solar wind monitoring to capture ICME impacts, irrespective of their visibility in solar imagery.

3.1. Dst Correlation with ICME Parameters: A key focus in space weather research involves correlating storm intensity, as measured by the Dst index minimum, with the properties of interplanetary coronal mass ejections (ICMEs), including speed, magnetic field strength, and orientation. The solar wind electric field, defined as the product of speed and the southward component of the interplanetary magnetic field (V·B_{south}), is widely regarded as the primary empirical driver of geomagnetic storms. O'Brien & McPherron (2000) demonstrated that the Dst index can be predicted by integrating V·B_{south} over time, indicating that faster ICMEs with stronger southward magnetic fields typically produce more intense storms. Supporting this, Richardson & Cane (2011, *Space Weather*) analyzed ICMEs from 1995–2009 and found that the likelihood of an ICME causing an intense geomagnetic storm increases with both its speed and magnetic field strength (Richardson & Cane, 2012a, 2012b). Their study revealed that nearly all ICMEs with a sustained southward B_z component of –10 nT or greater triggered at least moderate storms, while those with B_z < –20 nT frequently resulted in severe storms (Dst < –100 nT). However,

DOI: 10.63119/JEA15.2025

not all fast ICMEs produce major storms—magnetic field orientation plays a critical role, as evidenced by cases where fast ICMEs with predominantly northward fields caused only minor disturbances, whereas slower ICMEs with prolonged southward fields generated disproportionately strong storms.

The relationship between geomagnetic storm intensity, as measured by the Dst index, and interplanetary coronal mass ejection (ICME) parameters has been extensively studied. Statistically, the Dst minimum correlates reasonably well with the peak southward magnetic field (B) in the ICME or its sheath, and to a lesser extent with the ICME's speed. Zhang et al. (2008) analyzed intense-storm ICMEs and found that the Dst magnitude had a stronger correlation with the sheath's dynamic pressure and the ICME's internal southward magnetic flux than with CME speed alone—a finding supported by earlier studies such as Shodhan et al. (2000) and Wu & Lepping (2002), who demonstrated that stronger magnetic cloud fields and longer durations (often linked to larger ICME size) yield deeper Dst depressions. The RC dataset further reinforces these relationships, as evidenced by extreme cases such as the October 2003 Halloween ICME, which had an exceptionally high speed (~1800 km/s) and strong magnetic field (~56 nT), resulting in one of the lowest Dst values (–390 nT), compared to a moderate November 2001 event (B ~20 nT, speed ~700 km/s) that produced only a Dst of ~–100 nT. Additionally, Zhang et al. (2008) showed in their Figure 4 that larger ICMEs, in terms of radial width, tend to drive more intense storms, likely due to their prolonged disturbance duration. These findings align with recent work by Salice et al. (2023), further solidifying the understanding of ICME geoeffectiveness.

The Richardson–Cane model highlights the significant geoeffectiveness of both ICME ejecta and their associated sheaths, with approximately 50% of intense geomagnetic storms exhibiting a two-step profile due to contributions from the shock/sheath region (often driving the initial phase) followed by the ICME's internal southward field (Temmer et al., 2024). This dual influence was further supported by Tsurutani et al. (1988), who identified "shock sheath auroras" as evidence of sheath-driven auroral activity. The Richardson–Cane dataset reveals instances where turbulent sheath fields with strong southward components alone triggered intense storms (Dst < –100 nT), even without significant southward fields in the ICME itself. Conversely, slower ICMEs lacking shocks can still induce storms if their internal fields remain southward for prolonged periods, underscoring the complex interplay between sheath and ejecta dynamics in geomagnetic disturbances.

3.2. Multiple Dip Storms: A number of complex geomagnetic storms involve multiple coronal mass ejections (CMEs). As described by Richardson & Zhang (2008) in *Geophysical Research Letters (GRL)*, "multiple-step geomagnetic storms" occur when a series of CMEs in quick succession cause consecutive Dst dips. The Richardson and Cane (RC) catalog documents instances where one interplanetary CME (ICME) arrives immediately after another, such as the back-to-back ICMEs in August–September 2005 that produced a compound storm with two distinct minima (Richardson et al., 2016). Accurately identifying each ICME in such sequences is essential for interpreting the geomagnetic response, as the RC catalog often notes whether an ICME is followed by another shock or if two ICMEs have merged (Savani et al., 2016). These distinctions help prevent misattribution of storm phases to the correct solar wind structures, ensuring more precise space weather analysis.

3.3. Geomagnetic Indices in Catalog: The identification of geoeffective interplanetary coronal mass ejections (ICMEs) can be facilitated by referencing geomagnetic indices such as the *Dst* index or *Kp* index, which are often noted in catalogs with notations like "Dst = –150 nT" or "SC, Dst –50" to indicate storm magnitude, or "Kp=9" for extreme storms. A comprehensive analysis by Richardson & Cane (2011) examined geomagnetic activity (*Dst* and *Kp*) across four solar cycles (1963–2011), revealing that ICMEs are the primary drivers of severe space weather, with 10–20 ICMEs per solar cycle responsible for the most intense storms. Their findings, supported by earlier works (Tsurutani & Gonzalez, 1997; Richardson, 2013, 2014), demonstrate that ICMEs dominate geomagnetic activity during solar maximum, while co-rotating interaction regions (CIRs) contribute more during the declining phase and solar minimum. Crucially, their

DOI: 10.63119/JEA15.2025

research highlights that ICMEs are associated with approximately two-thirds of moderate storms (*Dst* < –50 nT) and ~90% of intense storms (*Dst* < –100 nT), whereas weaker disturbances (*Dst* > –30 nT) are often driven by high-speed streams alone. These insights underscore the importance of ICME detection in space weather forecasting.

3.4. Storm Forecasting Implications: The strong linkage between interplanetary coronal mass ejections (ICMEs) and geomagnetic storms has significant practical implications, as CME observations from the Sun—such as halo CMEs detected by coronagraphs—provide advance warnings for potential storms at Earth approximately 1–4 days later (Richardson & Cane, 2012a, 2012b). However, accurately forecasting storm intensity remains challenging due to the difficulty in predicting the ICME's magnetic field orientation, particularly the southward B_z component upon arrival. To address this, Savani et al. (2016) developed evolutionary models to predict CME magnetic vectors, leveraging historical ICME data from catalogs like the Richardson & Cane (RC) list for calibration. Similarly, Mays et al. (2015) employed ensemble modeling (WSA–ENLIL+Cone) to predict CME arrival times, achieving an average accuracy of ±6 hours for shock arrivals when validated against the RC catalog (Von Rosenvinge et al., 2009). Richardson & Cane (2011) further demonstrated the catalog's utility for probabilistic forecasting, showing that fast ICMEs with high Mach number shocks are more likely to trigger intense storms (Dst < –100), whereas slow ICMEs without shocks rarely produce significant disturbances—though exceptions, such as the May 1998 event, highlight the role of prolonged southward magnetic fields. Their findings underscore the limitations of relying solely on solar observations, as CMEs appearing large may only graze Earth, while smaller, head-on impacts with strong B_z can drive major storms. Consequently, databases like the RC catalog are indispensable for empirically based forecasting, as evidenced by studies such as Prikryl et al. (2012), which linked ICME occurrences to high-latitude GPS scintillations using probabilistic approaches.

3.5. Notable Events in the Catalog: The Richardson–Cane (RC) ICME catalog provides critical insights into the relationship between interplanetary coronal mass ejections (ICMEs) and geomagnetic storms, with several notable events serving as key case studies. Among these, the "Bastille Day" storm (14–16 July 2000) stands out—a fast (~1000 km/s) magnetic cloud with intense southward Bz triggered a superstorm (Dst –301 nT), demonstrating how a single ICME can produce extreme space weather under optimal conditions (one of the largest storms of Solar Cycle 23). Similarly, the Halloween Storms (October–November 2003) showcased the compounding effects of consecutive ICMEs, with three major events (e.g., Dst –350 to –400 nT on Oct 30) sustaining prolonged magnetospheric disturbance (Shodhan et al., 2000). The catalog also documents less obvious drivers, such as the "stealth" CME of June 8, 2012, which caused an unexpected storm (Dst ~–86 nT) despite lacking a clear solar eruption—later attributed to a faint CME (Nitta, 2021). Another well-studied case, the March 17, 2015 ICME, illustrates multiphase impacts: its shock (SSC at 04:45 UT) compressed the magnetopause, while sustained southward Bz drove a major storm (Dst –223 nT) and ultra-relativistic electron acceleration (Kanekal et al., 2016). Collectively, the RC catalog has solidified the understanding that ~90% of intense storms and nearly all superstorms are ICME-driven, a statistic now foundational to space weather frameworks. These findings directly inform predictive models and operational guidelines, such as NOAA's Space Weather Scales, which explicitly link the most severe storms to Earth-directed CMEs—a conclusion unequivocally supported by Richardson and Cane's work.

4.COSMIC RAY MODULATION BY ICMES

Beyond geomagnetic storms, ICMEs have a profound effect on galactic cosmic rays (GCRs) in the heliosphere. As an ICME (with its shock and magnetic structure) passes by, it can transiently reduce the intensity of cosmic rays observed at Earth – a phenomenon known as a Forbush decrease (FD). The Richardson–Cane ICME dataset, with its footnotes on cosmic ray observations, has been crucial for studying these events statistically and understanding the physical mechanisms behind them.

4.1. Forbush Decreases and ICMEs: A Forbush decrease (FD) is characterized by a sudden reduction

in cosmic ray intensity (typically a few percent for particles with rigidities ≳1 GV, as measured by neutron monitors), followed by a gradual recovery over days to weeks. Unlike the long-term 11-year solar cycle modulation, FDs are transient phenomena primarily driven by two solar wind structures: (1) corotating interaction regions (CIRs), which produce recurrent, often smaller-amplitude decreases tied to the Sun's 27-day rotation, and (2) interplanetary coronal mass ejection (ICME)-related disturbances, which cause nonrecurrent, larger-amplitude decreases associated with CME-driven shocks and ejecta (Farrugia et al., 2023; Wimmer-Schweingruber et al., 2006). Richardson & Cane (2011) analyzed over 300 ICMEs during solar cycle 23 (1995–2009) and found that ~80% of ICMEs produced a clear FD, while ~10% showed no significant change, and the remaining ~10% exhibited a slight cosmic ray increase—likely due to the Earth being at the ICME's edge or an ongoing recovery from a prior FD (Witasse et al., 2017; Wu & Lepping, 2002; Wu et al., 2007). Notably, when an FD occurred, the cosmic ray minimum almost always (≈90% of cases) coincided with the ICME's magnetic ejecta rather than the sheath or shock, underscoring the efficiency of the ICME's closed magnetic structure in excluding cosmic rays (Witasse et al., 2017; Yang et al., 2018). This supports a two-step FD profile, where the shock and sheath cause an initial partial decrease, followed by a further drop within the magnetic cloud—a pattern first qualitatively described by Wibberenz et al. (1998) and later quantified by Richardson & Cane.

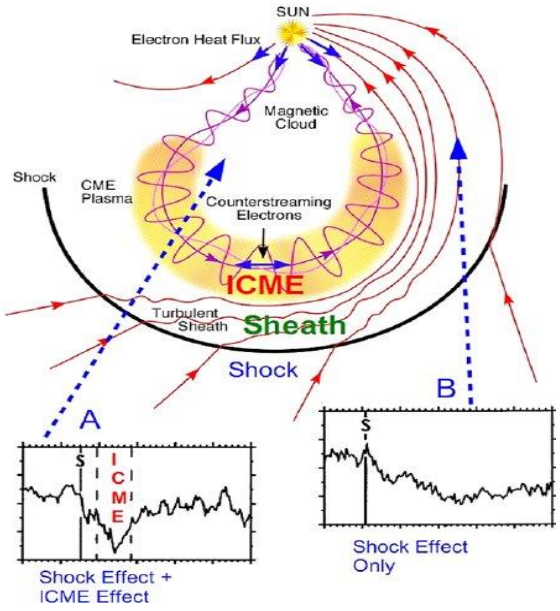

Figure 01. (adapted from Richardson & Cane, 2011) illustrates the two-step cosmic ray decrease for a trajectory encountering both a shock and an interplanetary coronal mass ejection (ICME). As demonstrated by Cane (2000) and Wimmer-Schweingruber et al. (2006), Path A (passing through the shock and ICME) exhibits a sharp drop at the shock due to a diffusion barrier in the sheath, followed by a further decrease inside the ICME before recovery upon exit (Zhang et al., 2007; Zhang et al., 2008). In contrast, Path B (skimming the shock but missing the ICME core) shows only a shock-related decrease with faster recovery (Cane, 2000). Observations from the Richardson & Cane (RC) catalog indicate that Earth's trajectories typically resemble Path A, resulting in the largest cosmic ray depressions inside the ICME. Their analysis separated the shock/sheath and ICME contributions to Forbush decreases (FDs), revealing that, on average, both contribute comparably to the total FD amplitude, though with significant case-by-case variability (Cane et al., 2000; Zurbuchen & Richardson, 2006). While some events were dominated by the turbulent sheath, others—particularly those involving large magnetic clouds—were primarily driven by the ICME itself. Key factors influencing FD magnitude include ICME speed, with faster, wider ICMEs producing larger decreases, whereas magnetic field strength and ICME size showed surprisingly weak direct correlations (Cane et al., 2000). Magnetically closed structures (e.g., magnetic clouds) tended to yield slightly larger FDs, though non-cloud ICMEs with strong shocks could also produce significant decreases. The RC catalog quantifies FD magnitudes using neutron monitor data (e.g., "~ –12% CR decrease (Thule NM)"), with typical ICME-related FDs ranging from a few percent up to ~20%. Extreme events, such as the March 1991 "Bastille" event (~20% drop), remain rare, while cycles with reduced ICME activity (e.g., Cycle 24) exhibit fewer and smaller FDs due to weaker heliospheric magnetic fields.

4.2. Radial and Rigidity Dependence: Forbush decreases (FDs) occur throughout the heliosphere, though the reference catalog (RC) list primarily focuses on near-Earth (1 AU) events. Multi-point observations, such as those by Witasse et al. (2017), demonstrate that FD magnitude generally diminishes with increasing heliocentric distance due to the

DOI: 10.63119/JEA15.2025

weakening effects of interplanetary coronal mass ejections (ICMEs). For instance, an ICME observed by Rosetta at 1.4 AU, Mars at 1.5 AU, and Saturn at ~9 AU exhibited this trend. Belov et al. (2023) further quantified this using Helios 1 and 2 data, confirming that FD percentage decreases are more pronounced at 0.3 AU than at 1 AU, aligning with diffusion models, as ICME magnetic fields and cosmic ray gradients are stronger closer to the Sun. Beyond Earth, FDs remain detectable at Mars or Jupiter, though with reduced amplitude unless the ICME retains significant strength. Additionally, cosmic ray energy dependence plays a critical role: high-energy particles (tens of GeV) experience smaller relative decreases, whereas lower-energy galactic cosmic rays (~1–5 GeV), detectable by neutron monitors, exhibit the largest fractional drops. Belov et al. (2021) analyzed FD energy spectra using neutron monitor and SOHO/EPHIN data (1–10 GV range), revealing rigidity-dependent spectral breaks or flattening linked to ICME structure—shocks affect a broader rigidity range, while magnetic clouds preferentially impact lower energies. These spectral studies, facilitated by the RC catalog's ICME identifications, enhance understanding of cosmic ray transport mechanisms, including diffusion coefficient variations across turbulent sheaths and quiescent flux ropes.

4.3. Long-Term Cosmic Ray Modulation: Interplanetary coronal mass ejections (ICMEs) not only produce short-term decreases in galactic cosmic ray (GCR) intensity but also cumulatively contribute to the 11-year solar modulation of cosmic rays. During solar maxima, frequent ICMEs and their merged effects—such as global disturbances propagating outward—result in lower overall GCR intensities, a phenomenon known as "solar maximum suppression." While steady-state modulation is typically modeled through variations in the heliospheric magnetic field and solar wind speed, ICMEs act as propagating barriers that further influence GCR flux. Richardson & Cane (2011) noted that the unusually high cosmic ray fluxes during the 2009 solar minimum were partially attributable to extremely low CME activity (and thus fewer transient barriers), alongside a weaker heliospheric field. As solar cycle 24 began, even its modest increase led to a corresponding drop in cosmic ray intensity, though levels remained higher than in previous maxima due to the reduced ICME frequency. Thus, ICMEs can be viewed as "spikes" superimposed on the broader modulation curve, yet their collective effect can lower the baseline GCR intensity. Modulation theory further incorporates phenomena like global merged interaction regions (GMIRs)—comprising amalgamated CME ejecta and shocks—to explain step-like decreases in cosmic ray intensity propagating outward (McKibben 1972; le Roux & Potgieter 1991). The Richardson & Cane (RC) list serves as a valuable timeline for identifying potential GMIR events in historical data.

4.4. Forbush Decrease Impacts and Uses: Forbush decreases (FDs), while primarily significant in cosmic ray physics, also hold notable practical implications. A sudden reduction in galactic cosmic ray (GCR) flux results in fewer high-energy particles penetrating Earth's atmosphere for brief periods, which has prompted research into potential atmospheric and climatic effects. Studies have explored whether FDs can influence cloud cover or atmospheric processes—termed the "Forbush decrease cloud effect"—leveraging FD events as natural experiments in cosmic ray-climate research (e.g., through the RC catalog, which aids in identifying periods of reduced cosmic ray flux). Some experiments have observed short-term variations in atmospheric ionization or aerosol properties coinciding with large FDs, though these findings remain debated. From a space radiation standpoint, FDs temporarily reduce cosmic ray exposure for spacecraft and astronauts; however, they often coincide with solar energetic particle (SEP) events from the originating coronal mass ejection (CME), potentially worsening the net radiation environment as SEP enhancements outweigh GCR reductions. For instance, the December 2006 event—analyzed by von Rosenvinge et al. (2009) and Munini et al. (2018)—demonstrated this duality, where a major CME triggered both a significant FD and an intense SEP storm, with the latter posing greater radiation risks despite the GCR dip.

4.5. Summary of RC Cosmic Ray Findings:

The ICME dataset has enabled a landmark statistical result, revealing that approximately 80% of ICMEs produce a measurable Forbush decrease (FD) at Earth, underscoring the prevalence of ICME–cosmic

ray interactions. The largest cosmic ray depressions occur when a strong magnetic cloud is present, with shock-ejecta combinations yielding the deepest decreases. A typical FD exhibits a rapid decline (~1 day) followed by a slower recovery (~days), reflecting the diffusion-driven replenishment of cosmic rays after the ICME passage. Notably, FDs serve as probes for solar wind diffusion coefficients, as demonstrated by Richardson & Cane (2011), who used a simple model linking FD magnitude to parameters such as magnetic field strength and ICME radius (with $K\perp$ representing the perpendicular diffusion coefficient). Their findings indicate that the effective perpendicular diffusivity within ICMEs is significantly lower than in the ambient solar wind (~10^{18}–10^{19} cm^2/s vs. ~10^{21} cm^2/s), consistent with the expectation that ICMEs' ordered magnetic fields and suppressed turbulence create a transient "cavity" that cosmic rays slowly refill. Observations from *Ulysses* further confirm that some ICMEs remain effective in reducing galactic cosmic rays (GCRs) even beyond 4 AU, indicating this phenomenon is not limited to near-Earth space.

In conclusion, ICMEs hold multidisciplinary significance, extending even to cosmic ray astrophysics. By cataloging ICMEs and their associated FDs, Richardson & Cane established a framework for systematically studying how solar transients modulate high-energy particle populations in the heliosphere. This reinforces the Sun-Earth system as not only electromagnetically connected but also dynamically coupled through particle radiation and diffusion processes.

Figure 01schematic illustrates an ICME at 1 AU driving a shock, with corresponding GCR intensity variations along two spacecraft trajectories. Trajectory A (passing through the shock/sheath and ICME) exhibits a two-step FD—a partial drop at the shock followed by a deeper decrease inside the ICME—before recovery. Trajectory B (grazing the ICME) shows only a minor decrease. This explains why ~80% of near-Earth ICMEs produce cosmic ray depressions, with minimum intensity typically occurring within the ICME itself (Adapted from Cane 2000; Zurbuchen & Richardson 2006; Richardson & Cane 2011).

5.SPACE WEATHER APPLICATIONS AND TECHNOLOGICAL IMPACTS

The Richardson–Cane ICME database has proved immensely valuable in operational space weather and in studies of how solar transients affect technological systems and planetary atmospheres. We highlight a few multidisciplinary benefits:

5.1. Space Weather Forecasting: Understanding the statistical behavior of interplanetary coronal mass ejections (ICMEs)—including their arrival frequency, transit times, and likelihood of triggering geomagnetic storms—is critical for enhancing space weather risk assessments. For instance, when NOAA issues a watch for an Earth-directed CME, the Richardson–Cane (RC) catalog provides empirical probabilities (e.g., a ~20% chance of a major storm for fast CMEs with specific characteristics). Probabilistic forecasting efforts, such as those by Prikryl et al. (2012), leverage ICME arrival data to predict subsequent ionospheric disturbances like GPS scintillation or geomagnetically induced currents. By analyzing past ICME events and their observed impacts (e.g., geomagnetic indices, radio blackouts), forecasters can refine predictive models with quantified confidence. The RC list also serves as a benchmark for validating CME arrival predictions, such as those from the WSA–ENLIL model, which estimates transit times with an average error of ±6–10 hours (Mays et al., 2015), driving iterative model improvements. Another key focus is predicting the ICME's magnetic field orientation (B_z), a critical factor in storm intensity. Statistical studies, like those by Riley et al. (2013), use the RC catalog to identify correlations between solar source properties (e.g., magnetic polarity, helicity) and observed B_z at Earth, though reliable predictive methods remain elusive. Additionally, "problem" storms—often caused by stealth CMEs or complex multi-CME events—highlight gaps in real-time detection, as noted by Nitta et al. (2021). The RC database confirms these overlooked events, prompting forecasters to enhance coronagraph techniques and integrate auxiliary data (e.g., heliospheric imagers) to improve detection accuracy.

5.2. Satellite Environment and Radiation Belts:

DOI: 10.63119/JEA15.2025

Interplanetary Coronal Mass Ejections (ICMEs), particularly those accompanied by shocks, exert complex and dynamic effects on Earth's radiation belts. The abrupt compression of the magnetosphere by an ICME-driven shock can lead to the depletion of high-energy "killer electrons" in the outer Van Allen belt or, conversely, trigger the acceleration of a new population of MeV electrons. Observations from the Van Allen Probes (2012–2019) have documented striking responses during ICME impacts, such as the March 2013 event studied by Kanekal et al. (2015), where the concurrent arrival of an ICME and a high-speed solar wind stream resulted in significant relativistic electron flux enhancements. Similarly, Kanekal et al. (2016) demonstrated that the March 17, 2015 ICME shock instantaneously accelerated electrons to ultrarelativistic energies (MeV) due to intense magnetospheric compression, providing critical insights into radiation belt dynamics under ICME-driven conditions. The Richardson & Cane (RC) catalog is frequently referenced in such studies to specify solar wind drivers, enabling engineers to correlate satellite anomalies with ICME or shock impacts—key indicators of high-energy particle environments or strong magnetopause currents. Satellite operators now recognize that ICME passages often coincide with heightened space weather hazards, including surface charging from enhanced particle fluxes and ionospheric disturbances that disrupt communications, underscoring the importance of real-time monitoring and predictive models for operational resilience.

5.3. Ground-Level Effects – Power Grids and Pipelines: Geomagnetically induced currents (GICs) in power grids are primarily driven by rapid geomagnetic field variations during storm-time substorms and sudden storm commencements (SSCs). Historical analysis reveals that the most severe GIC events, such as the Hydro-Québec blackout in March 1989, are associated with interplanetary coronal mass ejection (ICME)-driven superstorms. By cross-referencing the Richardson and Cane (RC) ICME catalog with ground-based GIC measurements, researchers have established that major GIC spikes coincide with ICME shock arrivals (SSCs) and intense magnetic cloud passages. Notably, the March 1989 storm—caused by an ICME not listed in the RC catalog due to its pre-1996 occurrence—and the October 2003 ICME-induced storms generated significant GICs in Scandinavian power grids. Studies such as Pulkkinen et al. (2017) have leveraged ICME catalogs to model geomagnetic disturbances and simulate GIC impacts, enabling retrospective risk assessments for utility providers. Beyond power grids, critical infrastructure like pipelines is also vulnerable, as GICs can accelerate corrosion rates. Industries reliant on such infrastructure benefit from ICME forecasting—for instance, by deploying pipeline current monitors that activate during predicted ICME events to mitigate potential damage.

5.4. Ionosphere and Communication Systems:

Interplanetary Coronal Mass Ejections (ICMEs) trigger geomagnetic storms that lead to significant ionospheric disturbances, disrupting high-frequency (HF) radio communications through D-region absorption during solar proton events and F-region scintillation during substorms. Additionally, GPS signals experience phase scintillation and range errors, particularly at high latitudes, as demonstrated by Prikryl et al. (2014), who conducted superposed epoch analyses of GPS phase scintillation around ICME and corotating interaction region (CIR) arrivals. Their findings revealed that ICME-driven storms enhance scintillation activity in the polar cap and auroral zones due to particle precipitation and intensified auroral electrojets, whereas high-speed stream arrivals produce a distinct scintillation pattern linked to recurrent substorm activity. These statistical studies, guided by ICME event lists, confirm that ICME-driven storms substantially impact navigation systems. Moreover, rapid fluctuations in ionospheric total electron content (TEC)—such as storm-enhanced density plumes—during ICME events further degrade GPS accuracy. Consequently, tracking ICME occurrences helps attribute GPS errors to ionospheric disturbances on specific dates, improving space weather forecasting and mitigation strategies.

5.5: Atmospheric and Climate Connections:

Recent interdisciplinary research has explored potential connections between solar storms and atmospheric processes, such as cloud microphysics and thunderstorms. While these investigations remain preliminary, one hypothesis suggests that

DOI: 10.63119/JEA15.2025

decreases in cosmic rays during Forbush events—temporary reductions in galactic cosmic ray flux caused by interplanetary coronal mass ejections (ICMEs)—may slightly reduce atmospheric ionization and cloud nucleation, providing a test for cosmic ray-climate theories. Studies such as Svensmark et al. (2016) have examined cloud cover variations following significant Forbush decreases (FDs), relying on event catalogs like the RC catalog to identify FD timings and magnitudes. Although findings have been inconsistent, some analyses observed minor, short-lived changes in aerosol or cloud parameters following the most intense ICME-driven FDs. This area of study remains contentious, yet it demonstrates how solar-terrestrial datasets can extend into atmospheric science and other disciplines, offering intriguing avenues for further research.

5.6. Other Planetary Space Weather:

The RC catalog, primarily focused on near-Earth phenomena, has inspired analogous efforts for other planetary environments, such as the catalog of ICMEs at Mercury derived from MESSENGER data (Winslow et al., 2015) and studies of ICMEs at Mars (Liu et al., 2014). By leveraging Earth's ICME records alongside observations from missions like STEREO or MSL/Curiosity at Mars, researchers such as Palmerio et al. (2022) investigate the evolution of ICMEs across different heliospheric distances and their varying impacts at multiple locations, with Earth's data serving as a critical reference point. Additionally, multispacecraft analyses (Witasse, 2017; Lario, 2022) spanning from Earth to the outer planets frequently rely on the RC catalog for accurate Earth-encounter timings and ICME characteristics. This cross-planetary calibration is essential for advancing our understanding of ICME propagation, deceleration, and the spatial broadening of their effects with increasing heliocentric distance.

5.7. Human Spaceflight Considerations:

During ICME-driven solar storms, astronauts aboard the International Space Station (ISS) or future lunar and Martian missions must remain vigilant for heightened radiation levels caused by solar energetic particle (SEP) events and seek shelter when necessary. The shock front of an interplanetary coronal mass ejection (ICME) can accelerate SEPs, as observed in historical events like the August 1972 storm, where particles arrived abruptly with the shock. The Richardson–Cane ICME catalog identifies such events with an "SEP" designation, providing critical data to inform mission protocols—for instance, prompting crews to prepare for both ICME impacts and potential SEP storms following a fast CME detection. Beyond academic research, the catalog plays a pivotal role in modern space weather forecasting, enhancing our comprehension of solar-terrestrial interactions and their technological impacts. By meticulously documenting ICMEs and their downstream effects, the catalog offers a comprehensive perspective, tracing the Sun's influence from its corona through interplanetary space to Earth's environment, thereby strengthening operational readiness and risk mitigation strategies.

CONCLUSION

The Near-Earth Interplanetary CME Dataset (1996–2024), compiled by Richardson and Cane, represents a foundational long-term dataset that has significantly advanced both scientific understanding and practical applications in heliophysics. Spanning nearly three solar cycles, this catalog meticulously documents Earth-directed interplanetary coronal mass ejections (ICMEs), capturing the Sun's explosive activity and its impact on our planet. By aggregating these events, the dataset has revealed critical patterns—such as the correlation between ICME frequency and solar cycle dynamics—that would be impossible to discern from isolated observations. Notably, it has quantified key phenomena, including the 150-day quasi-periodicity in solar output and the differences in ICME properties between Solar Cycle 23 (more frequent, faster, and magnetically stronger events) and the weaker Cycle 24. These insights align with broader trends in solar magnetism, reinforcing the dataset's scientific value.

Scientific and Operational Impact

The Richardson–Cane catalog has become indispensable for space physics research, providing robust statistics such as the finding that ~90% of intense geomagnetic storms are ICME-driven, while ~80% of ICMEs trigger Forbush decreases in cosmic ray flux. These metrics are now foundational in space

DOI: 10.63119/JEA15.2025

weather studies. Additionally, the dataset serves as a critical validation tool for space missions like STEREO, Parker Solar Probe, and Solar Orbiter, enabling researchers to compare remote or in-situ CME observations with near-Earth measurements. This cross-validation has enhanced our understanding of CME propagation, including deflection, expansion, and interaction with solar wind structures—knowledge that directly improves predictive modeling. Beyond research, the catalog is deeply embedded in operational space weather monitoring, with agencies like NASA, NOAA, and ESA routinely referencing it for post-event analyses and training purposes.

Cross-Disciplinary and Future Applications

A key strength of the Richardson–Cane dataset lies in its ability to bridge multiple disciplines, connecting solar physics, heliospheric dynamics, magnetospheric studies, and even cosmic ray astrophysics. Solar researchers use it to correlate flare properties with ICME geoeffectiveness, while magnetospheric scientists leverage it to analyze radiation belt responses. Looking ahead, as Solar Cycle 25 intensifies, the catalog is expected to expand with new ICME entries, aided by advanced observational capabilities from missions like Solar Orbiter and DSCOVR. Future enhancements may include richer annotations, such as links to solar energetic particle (SEP) events or heliospheric imager tracking. Maintaining this dataset over the long term will enable investigations into century-scale solar variability, including potential Grand Minimum periods and shifts in CME productivity across solar cycles.

The period from 2026 to 2030 marks the transition of Solar Cycle 25 from its peak into its declining phase. While the overall frequency of Interplanetary Coronal Mass Ejections (ICMEs) and space weather events will gradually decrease following the 2025-2026 solar maximum, the potential for significant impacts remains. The early part of this window, particularly from late 2026 through 2028, is poised to present an elevated risk of some of the cycle's most intense geomagnetic storms. This heightened risk arises from the increased prevalence of powerful, geo-effective CMEs from the Sun's equatorial regions and the potential for complex ejecta as faster ICMEs interact with slower solar wind. However, a clear shift will occur as the cycle progresses towards its minimum around 2029-2030, with space weather activity transitioning to a lower rate of more isolated, and typically less severe, events. Despite being a stronger cycle than initially forecast, Solar Cycle 25's overall weaker-than-average strength compared to historical cycles will ultimately lead to a significant decline in both the frequency and intensity of major geomagnetic storms by the end of the decade.

Expanding the Legacy

The dataset's influence may extend beyond Earth, inspiring similar ICME catalogs for other planets as human and robotic exploration advances. For instance, with Artemis missions targeting the Moon and future crewed deep-space missions, tracking ICMEs throughout the inner solar system will be vital for radiation safety. Similarly, studying ICME impacts on Mars—where the lack of a global magnetic field leads to distinct atmospheric effects—could provide new insights into planetary space weather.

The Richardson and Cane ICME catalog exemplifies the transformative power of systematic, long-term data collection. It has driven discoveries in solar-heliospheric physics, refined space weather forecasting, and informed mitigation strategies for technological systems. Its open availability via the Harvard Dataverse ensures continued accessibility and community engagement. As we move forward, sustaining such efforts—potentially augmented by machine learning while retaining expert oversight—will remain essential for advancing space science. The scientific community owes a profound debt to Richardson and Cane for their decades of meticulous work, which has not only deepened our understanding of solar-terrestrial connections but also underscored the Sun's far-reaching influence on our technologically dependent world.

REFERENCES

1.Belov, A., Baisultanova, L., Eroshenko, E., Malkov, M., & Yanke, V. (2021). On the rigidity spectrum of cosmic-ray variations within propagating interplanetary disturbances: Neutron monitor and SOHO/EPHIN observations at ~1–10 GV. Astrophysical Journal, 910(1), 8.

2. Belov, A., Eroshenko, E., Oleneva, V., Struminsky, A., Yanke, V., & Abunina, M. (2023). Study of the radia dependence of Forbush

decreases at 0.28–1 AU using data from the Helios 1 and 2 spacecraft. Monthly Notices of the Royal Astronomical Society, 519(3), 3935–3943.

3.Bruno, A., Christian, E. R., de Nolfo, G. A., Lave, K. A., Mewaldt, R. A., Richardson, I. G., & Ryan, J. M. (2019). Spectral analysis of the September 2017 solar energetic particle events. Space Weather, 17(8), 1193–1208.

4.Cane, H. V. (2000). Coronal mass ejections and Forbush decreases. Space Science Reviews, 93(1/2), 55–77.

5.Cane, H. V., & Lario, D. (2006). An introduction to CMEs and energetic particles. Space Science Reviews, 123(1–3), 45–56.

6.Cane, H. V., & Richardson, I. G. (2003). Interplanetary coronal mass ejections in the near-Earth solar wind during 1996–2002. Journal of Geophysical Research: Space Physics, 108(A4), 1156.

7.Cane, H. V., Richardson, I. G., & St Cyr, O. C. (2000). Coronal mass ejections, interplanetary ejecta and geomagnetic storms. Geophysical Research Letters, 27(21), 3591–3594. 86 54

8.Cane, H. V., Richardson, I. G., & von Rosenvinge, T. T. (1993). Cosmic ray decreases and particle acceleration in 1978–1982 and the associated solar wind structures. Journal of Geophysical Research: Space Physics, 98(A9), 13295–13305.

9.Cane, H. V., Richardson, I. G., von Rosenvinge, T. T., & Wibberenz, G. (1994). Cosmic ray decreases and shock structure: A multi-spacecraft study. Journal of Geophysical Research: Space Physics, 99(A11), 21429–21441.

10.Cliver, E. W., Tiwari, S. K., Petrie, G. J. D., & Richardson, I. G. (2024). A floor in the Sun's photospheric magnetic field: Implications for an independent small-scale dynamo. Astrophysical Journal Letters, 940(1), L6.

11.Farrugia, C. J., Burlaga, L. F., Lepping, R. P., et al. (1993a). Simultaneous observations of solar MeV particles in a magnetic cloud and in the Earth's northern tail lobe: Implications for the global field line topology of magnetic clouds and for the entry of solar particles into the magnetosphere during cloud passage. Journal of Geophysical Research: Space Physics, 98(A9), 15497–15507.

12.Farrugia, C. J., Osherovich, V. A., Burlaga, L. F., et al. (1993b). A study of an expanding interplanetary magnetic cloud and its interaction with the Earth's magnetosphere: The interplanetary aspect. Journal of Geophysical Research: Space Physics, 98(A5), 7621–7632.

13.Farrugia, C. J., Berdichevsky, D. B., & Ogilvie, K. W. (2023). How magnetic reconnection may affect the coherence of interplanetary coronal mass ejections. Astrophysical Journal, 949(2), 92.

14.Forsyth, R. J., Burlaga, L. F., Oneill, C., et al. (2006). ICMEs in the inner heliosphere: Origin, evolution and propagation effects. Space Science Reviews, 123(1–3), 383–416.

15.Gopalswamy, N. (2006). Coronal mass ejections: An introduction. In Solar Eruptions and Energetic Particles, *Geophysical Monograph 165 (pp. 207–220).*

16.Howard, T. A. (2011). Coronal Mass Ejections: An Introduction. *Springer. DOI 10.1007/978-1-4419-8789-1*

17.Howard, T. A. (2014). Space Weather and Coronal Mass Ejections. *Springer.*

18.Iucci, N., Parisi, M., Storini, M., & Villoresi, G. (1989). Forbush decreases: Energetic particle propagation and magnetic cloud geometry. In 25th International Cosmic Ray Conference, *Vol. 3 (pp. 65–68).*

19.Jian, L. K., Russell, C. T., Luhmann, J. G., & Galvin, A. B. (2018). Solar wind observations and ICME identifications at STEREO. Astrophysical Journal, 855(2), 114.

20.Kahler, S. W., Haggerty, D. K., & Richardson, I. G. (2011). Magnetic field-line lengths in interplanetary coronal mass ejections inferred from energetic electron events. Astrophysical Journal, 736(2), 106.

21.Kanekal, S. G., Li, X., Schiller, Q., et al. (2015). Relativistic electron response to the combined magnetospheric impact of a coronal mass ejection overlapping with a high-speed stream: Van Allen Probes observations. Journal of Geophysical Research: Space Physics, 120(9), 7626–7636.

22.Kanekal, S. G., Baker, D. N., Pulkkinen, A., et al. (2016). Prompt acceleration of magnetospheric electrons to ultrarelativistic energies by the 17 March 2015 interplanetary shock. Journal of Geophysical Research: Space Physics, 121(8), 7622–7635.

23.Klein, L. W., & Burlaga, L. F. (1982). Interplanetary magnetic clouds at 1 AU. Journal of Geophysical Research: Space Physics, 87(A2), 613–624.

24.Lepping, R. P., Jones, J. A., & Burlaga, L. F. (1990). Magnetic field structure of interplanetary magnetic clouds at 1 AU. Journal of Geophysical Research: Space Physics, 95(A8), 11957–11965.

25.Lepri, S. T., Zurbuchen, T. H., Fisk, L. A., et al. (2001). Iron charge distribution as an identifier of interplanetary coronal mass ejections. Journal of Geophysical Research: Space Physics, 106(A12), 29231–29238.

26.Liou, K., Zhang, Y., Temerin, M., et al. (2017). Substorm occurrence and intensity associated with three types of solar wind structure. Journal of Geophysical Research: Space Physics, 122(5), 5431–5447.

27.Liu, Y., Richardson, J. D., & Belcher, J. W. (2005). A statistical study of the properties of interplanetary coronal mass ejections from 1979 to 1988. Planetary and Space Science, 53(1–3), 3–17.

28.Liu, Y. D., Richardson, J. D., Belcher, J. W., Kasper, J. C., & Elliott, H. A. (2006). Thermodynamic structure of collision-dominated expanding plasma: Heating of interplanetary coronal mass ejections. Journal of Geophysical Research: Space Physics, 111(A7), A07S03.

29.Mays, M. L., Taktakishvili, A., Pulkkinen, A., et al. (2015). Ensemble modeling of CMEs using the WSA– ENLIL+Cone model. Solar Physics, 290(6), 1775–1814.

30.Munini, R., Bruno, A., Füßling, M., et al. (2018). Evidence of energy and charge sign dependence of the recovery time for the 2006 December Forbush event measured by the PAMELA experiment. Astrophysical Journal, 853(1), 76.

31.Nitta, N. V., Mulligan, T., Wrobel, J. M., et al. (2021). Understanding the origins of problem geomagnetic storms associated with "stealth" coronal mass ejections. Space Science Reviews, 217(5), 77.

32.Ogunmodimu, O., Rabiu, B. A., & Chukwuma, V. U. (2020). Empirical modeling of auroral absorption during disturbed periods of interplanetary coronal mass ejection events. Journal of Atmospheric and Solar-Terrestrial Physics, 205, 105290.

33.Palmerio, E., Kilpua, E. K. J., Pomoell, J., et al. (2022). CME evolution in the structured heliosphere and effects at Earth and Mars during solar minimum. Space Weather, 20(11), e2022SW003086.

34.Prikryl, P., Jayachandran, P. T., Mushini, S. C., & Richardson, I. G. (2012). Toward the probabilistic forecasting of high-latitude GPS phase scintillation. Space Weather, 10(8), S08005.

35.Prikryl, P., Jayachandran, P. T., Mushini, S. C., & Richardson, I. G. (2014). High-latitude GPS phase scintillation and cycle slips during high-speed solar wind streams and interplanetary coronal mass ejections: A superposed epoch analysis. Earth, Planets and Space, 66, 62.

36.Riley, P., Lionello, R., Linker, J. A., et al. (2006). Rates of coronal mass ejections: A quantitative comparison of coronal and in situ observations. Astrophysical Journal, 647(1), 648–653.

37.Riley, P., & Richardson, I. G. (2013). Using statistical multivariable models to understand the relationship between interplanetary coronal mass ejecta and magnetic flux ropes. Solar Physics, 284(1), 217–231.

38.Richardson, I. G. (1994). A survey of bidirectional ≥ 1 MeV ion flows during the HELIOS 1 and 2 missions: Observations from the Goddard Space Flight Center instruments. Astrophysical Journal Supplement Series, 90,
629–647.

39.Richardson, I. G. (2013). Geomagnetic activity during the rising phase of solar cycle 24. Journal of Space Weather and Space Climate, 3, A08.

40.Richardson, I. G. (2014). Identification of interplanetary coronal mass ejections at Ulysses using multiple solarwind signatures. Solar Physics, 289(8), 3843–3894.

41.Richardson, I. G., & Cane, H. V. (1993). Signatures of shock drivers in the solar wind and their dependence on the solar source location. Journal of Geophysical Research: Space Physics, 98(A9), 15295–15304.

42.Richardson, I. G., & Cane, H. V. (1995). Regions of abnormally low proton temperature in the solar wind (1965– 1991) and their association with ejecta. Journal of Geophysical Research: Space Physics, 100(A12), 23397–
23412.

43.Richardson, I. G., & Cane, H. V. (1996). Particle flows observed in ejecta during solar event onsets and their implication for the magnetic field topology. Journal of Geophysical Research: Space Physics, 101(A11), 27521– 27533.

44.Richardson, I. G., & Cane, H. V. (1997). A statistical study of the behavior of the electron temperature in ejecta. Journal of Geophysical Research: Space Physics, 102(A7), 14683–14692.

45.Richardson, I. G., & Cane, H. V. (1999). Bidirectional ~1 MeV ion flows observed by IMP 8 over two solar cycles. In Proceedings of the 26th International Cosmic Ray Conference (Vol. 6, pp. 344–347).

46.Richardson, I. G., & Cane, H. V. (2004a). Identification of interplanetary coronal mass ejections at 1 AU using multiple solar wind plasma composition anomalies. Journal of Geophysical Research: Space Physics, 109(A9), A09104.

47.Richardson, I. G., & Cane, H. V. (2004b). The fraction of interplanetary coronal mass ejections that are magnetic clouds: Evidence for a solar cycle variation. Geophysical Research Letters, 31(18), L18804.

48.Richardson, I. G., & Cane, H. V. (2005). The ~150-day quasi-periodicity in interplanetary and solar phenomena during cycle 23. Geophysical Research Letters, 32(2), L02104.

49.Richardson, I. G., & Cane, H. V. (2007). Interplanetary coronal mass ejections during 1996–2007. In Proceedings of the 30th International Cosmic Ray Conference (Vol. 1, pp. 129–132).

50.Richardson, I. G., & Cane, H. V. (2008). Multiple-step geomagnetic storms and their interplanetary drivers. Geophysical Research Letters, 35(6), L06104.

51.Richardson, I. G., & Cane, H. V. (2010a). Near-Earth interplanetary coronal mass ejections during solar cycle 23 (1996–2009): Catalog and summary of properties. Solar Physics, 264(1), 189–237.

52.Richardson, I. G., & Cane, H. V. (2010b). The interplanetary circumstances of quasi-perpendicular interplanetary shocks in 1996–2005. Journal of Geophysical Research: Space Physics, 115(A7), A07103.

53.Richardson, I. G., & Cane, H. V. (2011a). Galactic cosmic ray intensity response to interplanetary coronal mass ejections/magnetic clouds in 1995–2009. Solar Physics, 270(2), 609–627.

54.Richardson, I. G., & Cane, H. V. (2011b). Geoeffectiveness (Dst and Kp) of interplanetary coronal mass ejections during 1995–2009 and implications for storm forecasting. Space Weather, 9(7), S07005.

55.Richardson, I. G., & Cane, H. V. (2012a). Solar wind drivers of geomagnetic storms during more than four solar cycles. Journal of Space Weather and Space Climate, 2, A01.

56.Richardson, I. G., & Cane, H. V. (2012b). Near-Earth solar wind flows and related geomagnetic activity during more than four solar cycles (1963–2011). Journal of Space Weather and Space Climate, 2, A02.

57.Richardson, I. G., Cliver, E. W., Cane, H. V., et al. (2000). Bidirectional particle flows at cosmic ray and lower (~1 MeV) energies and their association with interplanetary coronal mass ejections/ejecta. Journal of Geophysical Research: Space Physics, 105(A8), 18203–18213.

58.Richardson, I. G., Farrugia, C. J., & Burlaga, L. F. (1991). Energetic ion observations in the magnetic cloud of 14–15 January 1988 and their implications for the magnetic field topology. In Proceedings of the 22nd International Cosmic Ray Conference (Vol. 3, pp. 85–88).

59. The properties of solar energetic particle eventassociated coronal mass ejections reported in different CME catalogs. Solar Physics, 290(6), 1741–1759.

60.Richardson, I. G., von Rosenvinge, T. T., & Cane, H. V. (2016). North–south hemispheric periodicities in the >25 MeV solar proton event rate during the rising and peak phases of solar cycle 24. Solar Physics, 291(7), 2117–2135.

61.Salice, J., Schiller, Q., & Li, X. (2023). Exploring the predictability of the high-energy tail of MEE precipitation based on solar wind properties. Journal of Geophysical Research: Space Physics, 128(5), e2022JA031001.

62.Savani, N. P., Szabo, A., Kuchar, T., et al. (2016). Predicting the magnetic vectors within coronal mass ejections arriving at Earth: 2. Geomagnetic response. Space Weather, 14(10), 706–714.

63.Shodhan, S., Crooker, N. U., Kahler, S. W., et al. (2000). Counterstreaming electrons in magnetic clouds. Journal of Geophysical Research: Space Physics, 105(A12), 27261–27268.

64.Temmer, M., Reiss, M. A., Möstl, C., et al. (2024). CME propagation through the heliosphere: Status and future of observations and model development. Advances in Space Research, 73(1), 74–96.

65.Tsurutani, B. T., & Gonzalez, W. D. (1997). The interplanetary causes of magnetic storms: A review. In Magnetic Storms, Geophysical Monograph 98 (pp. 77–89).

66.von Rosenvinge, T. T., Richardson, I. G., Reames, D. V., et al. (2009). The solar energetic particle event of 14 December 2006. Solar Physics, 256(1–2), 443–462.

67.Wimmer-Schweingruber, R. F., Crooker, N. U., Balogh, A., et al. (2006). Understanding interplanetary coronal mass ejection signatures. Space Science Reviews, 123(1–3), 177–216.

68.Witasse, O., Sánchez-Cano, B., Mays, M. L., et al. (2017). Interplanetary coronal mass ejection observed at STEREO-A, Mars, comet 67P/Churyumov-Gerasimenko, Saturn, and New Horizons en route to Pluto: Comparison of its Forbush decreases at 1.4, 3.1, and 9.9 AU. Journal of Geophysical Research: Space Physics, 122(8), 7865–7890.

69.Wu, C. C., & Lepping, R. P. (2002). Effects of magnetic clouds on cosmic rays: Cosmic ray modulation by magnetic clouds. Journal of Geophysical Research: Space Physics, 107(A8), 1214.

70.Wu, C. C., Fry, C. D., Wu, S. T., Dryer, M., & Liou, K. (2007). Three-dimensional global simulation of interplanetary coronal mass ejection propagation from the Sun to the heliosphere: Solar event of 12 May 1997. Journal of Geophysical Research: Space Physics, 112(A9), A09104.

71.Yang, Z., Li, M., Wang, X., Tang, Y., & Zhuang, B. (2018). Correlation between the magnetic field and plasma parameters at 1 AU. Solar Physics, 293, 95.

72.Zhang, J., Richardson, I. G., Webb, D. F., et al. (2007). Solar and interplanetary sources of major geomagnetic storms (Dst < –100 nT) during 1996–2005. Journal of Geophysical Research: Space Physics, 112(A10), A10102.

73.Zhang, J., & Richardson, I. G. (2008). Multiple-step geomagnetic storms and their interplanetary drivers.
Geophysical Research Letters, 35(6), L06104.

74.Zhang, J., Poomvises, W., & Richardson, I. G. (2008). Sizes and relative geoeffectiveness of interplanetary
coronal mass ejections and the preceding shock sheaths during intense storms in 1996–2005. Geophysical
Research Letters, 35(2), L02109.

75.Zurbuchen, T. H., & Richardson, I. G. (2006). In-situ solar wind and magnetic field signatures of interplanetary
coronal mass ejections. Space Science Reviews, 123(1–3), 31–43.

DOI: 10.63119/JEA15.2025

APPENDIX

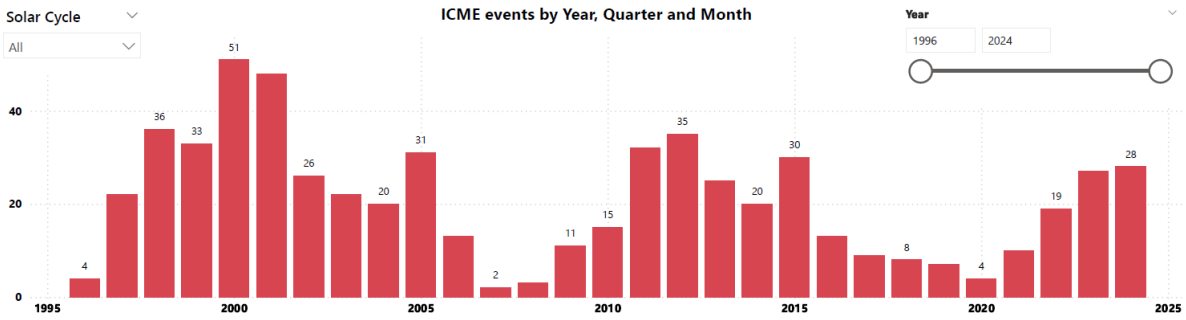

Figure 02: Annual distribution of Interplanetary Coronal Mass Ejection (ICME) events from 1996 to 2024, with counts aggregated by year. © Eco Astronomy Inc 2025.

This figure illustrates the temporal variation of ICME events across the period 1996–2024. The frequency of events shows strong fluctuations, with peaks around the years 2000, 2002, 2012, and 2015, coinciding with solar cycle maxima. Event counts diminish during solar minima, highlighting the cyclical nature of solar activity. The most active year in this interval is 2000, recording 51 ICME events, while periods of low activity (e.g., 2008–2009 and 2020–2021) exhibit fewer than 10 events annually. This pattern reinforces the established relationship between solar cycle progression and interplanetary CME occurrence.

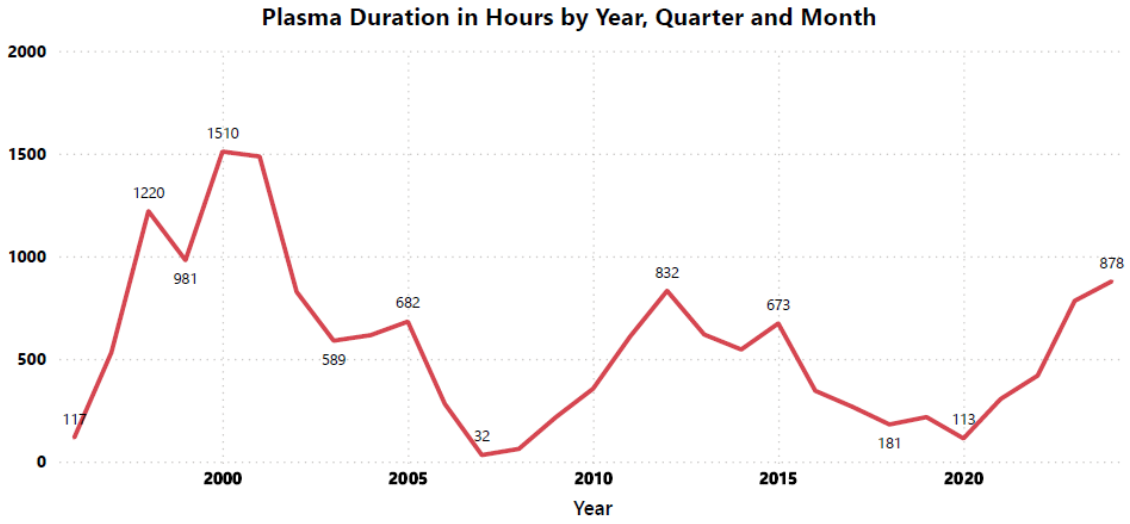

Figure 03: Annual variation of ICME-associated plasma duration (in hours) from 1996 to 2024, aggregated by year, quarter, and month. © Eco Astronomy Inc 2025.

This figure presents the yearly trend of plasma durations linked to ICME events between 1996 and 2024. The data reveal substantial fluctuations, with prolonged plasma intervals during solar cycle maxima, peaking in 2000 at 1,510 hours. Extended durations are also evident in 1999 (1,220 hours) and 2011 (832 hours), while markedly reduced activity is observed in 2006 (32 hours) and 2020 (113 hours). The overall pattern reflects the influence of solar cycle dynamics, with high plasma durations coinciding with enhanced ICME activity and significantly shorter durations during solar minima.

DOI: 10.63119/JEA15.2025

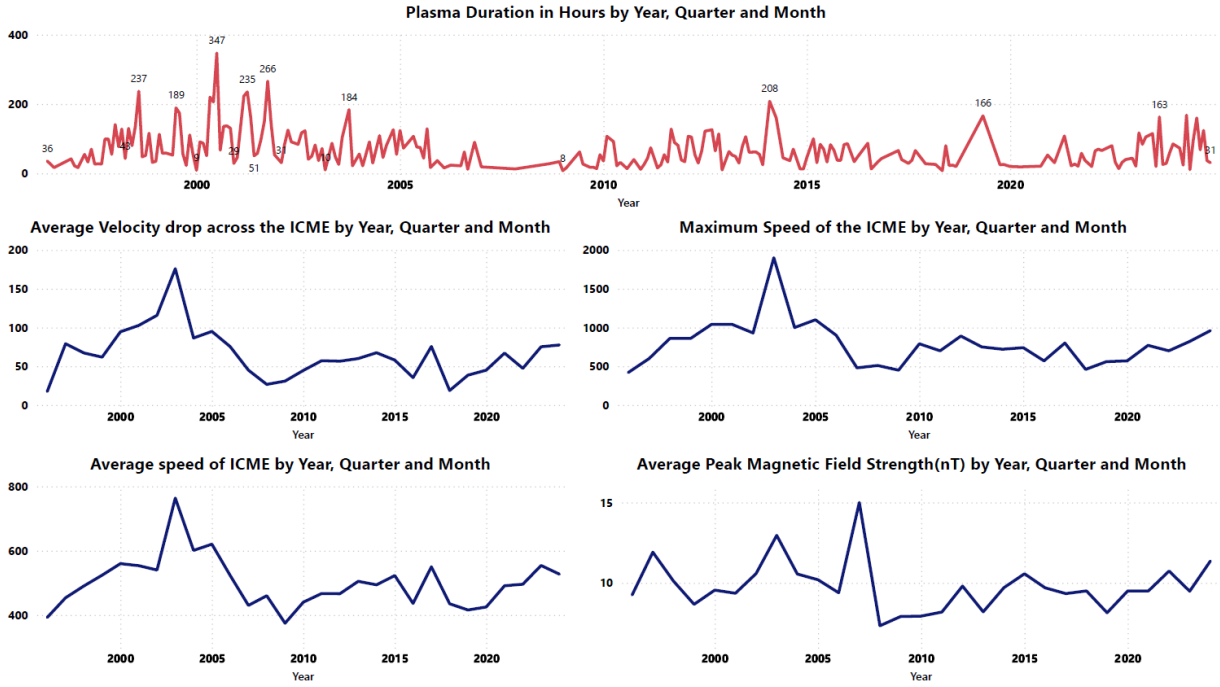

Figure 04: Temporal variation of key ICME plasma and magnetic field parameters from 1996 to 2024, aggregated by year, quarter, and month. © Eco Astronomy Inc 2025.

This figure summarizes multiple characteristics of interplanetary coronal mass ejections (ICMEs) over the period 1996–2024. Plasma duration (top panel) shows highly variable intervals, with spikes exceeding 300 hours during solar maxima (e.g., 2000 and 2012), and significantly shorter durations near solar minima. The average velocity drops across ICMEs (bottom left) peaks around 2003, reflecting strong deceleration during periods of intense solar activity. The maximum ICME speed (top right) reached its highest levels above 1,800 km/s in the early 2000s, while average ICME speeds (bottom left) remained between 400–800 km/s, with a notable peak around 2002–2003. The average peak magnetic field strength (bottom right) generally fluctuates between 8–12 nT, with pronounced enhancements above 15 nT during 2006 and other solar active phases. Together, these parameters illustrate the cyclical dependence of ICME properties on solar activity, highlighting the complex interplay between plasma dynamics and magnetic field intensities across solar cycles.

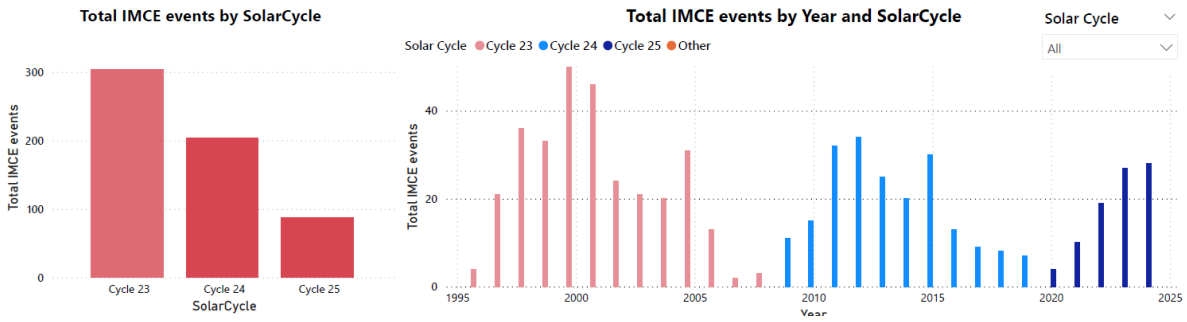

Figure 05: Total ICME events categorized by solar cycles (23–25) and their yearly distribution from 1996 to 2024. © Eco Astronomy Inc 2025.

The left panel shows the cumulative number of ICME events across solar cycles, with Cycle 23 (1996–2008) recording the highest activity (~300 events), followed by Cycle 24 (~200 events), and Cycle 25 (ongoing) showing fewer events to date. The right panel illustrates the yearly distribution of ICMEs within each cycle, highlighting peak activity during the maxima of Cycle 23 (around 2000–2002) and Cycle 24 (2011–2014). The gradual increase in Cycle 25 activity after 2020 suggests a rising trend toward its maximum phase. Overall, the results demonstrate the strong dependence of ICME occurrence rates on solar cycle progression, with distinct peaks aligning with solar maxima and reduced activity during minima.

DOI: 10.63119/JEA15.2025

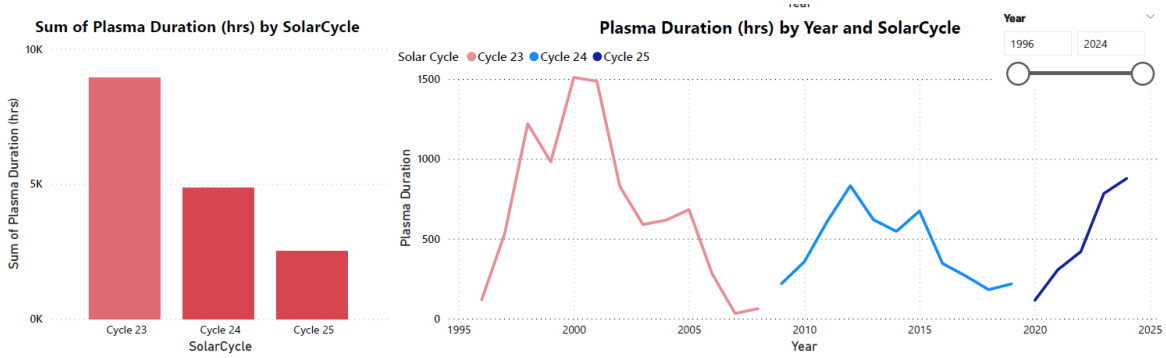

Figure 06: Total and yearly distribution of ICME plasma duration (in hours) across solar cycles 23–25 (1996–2024). © Eco Astronomy Inc 2025.

The left panel shows the cumulative plasma duration across solar cycles, with Cycle 23 contributing the largest total (>9,000 hours), followed by Cycle 24 (~5,000 hours) and the ongoing Cycle 25 (~2,500 hours to date). The right panel illustrates the year-by-year variation of plasma duration within each cycle. Plasma intervals were longest during Cycle 23, peaking near 2000 with durations exceeding 1,500 hours, and moderately high during Cycle 24, particularly around 2011–2012. Cycle 25, while still in progress, shows a rising trend in plasma duration since 2020, consistent with the approach toward its solar maximum. These results highlight the cyclical modulation of plasma durations, with maxima aligning closely with phases of heightened solar activity.

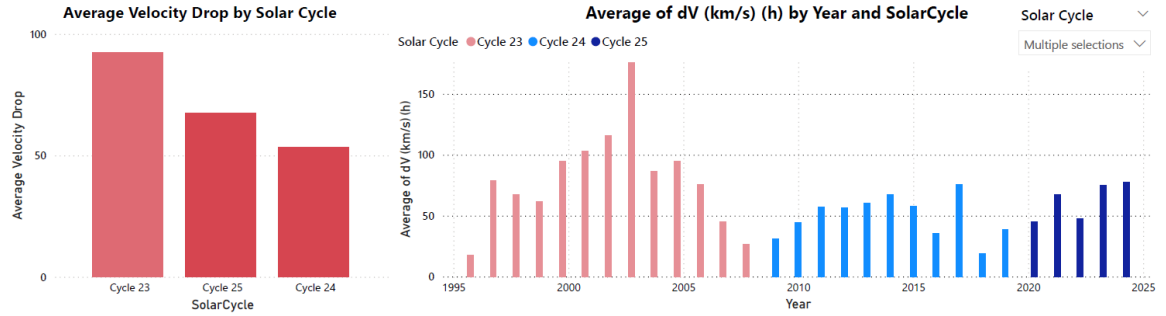

Figure 07: Average ICME velocity drop (ΔV) by solar cycle and its yearly distribution from 1996 to 2024. © Eco Astronomy Inc 2025.

The left panel compares the average ICME velocity drop across solar cycles, showing the largest deceleration during Cycle 23 (~90 km/s), followed by Cycle 25 (~70 km/s to date), and the lowest in Cycle 24 (~55 km/s). The right panel presents the annual distribution of ΔV, with strong deceleration episodes in the early 2000s, peaking above 170 km/s around 2003. In contrast, Cycle 24 exhibited lower and more stable values, while Cycle 25 shows a gradual increase since 2020, suggesting intensification as solar activity rises toward its maximum. These results indicate that ICME deceleration is strongly modulated by solar cycle phase, with the most pronounced velocity drops occurring during active periods of solar maxima.

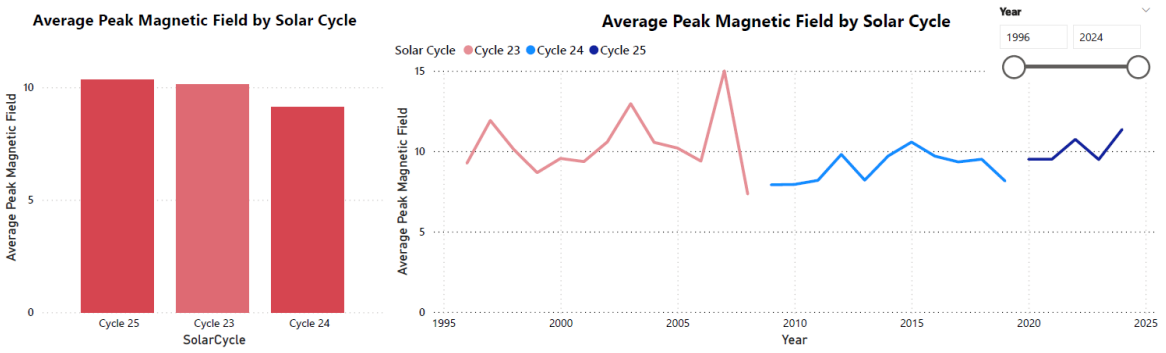

Figure 08: *Average peak magnetic field strength of ICMEs by solar cycle and its yearly distribution from 1996 to 2024.* © Eco Astronomy Inc 2025.

The left panel shows the cycle-averaged peak magnetic field strengths of ICMEs, with Cycle 25 (~10.5 nT) slightly higher than Cycle 23 (~10.2 nT) and Cycle 24 (~9 nT). The right panel highlights the yearly variability, with strong enhancements above 12 nT during 1997–1998 and 2003, and a pronounced peak of ~15 nT in 2006. During Cycle 24, values remained relatively stable near 9–10 nT, while early observations from Cycle 25 indicate a modest upward trend since 2020. These results suggest that, although Cycle 24 exhibited weaker magnetic fields compared to neighboring cycles, Cycle 25 is trending toward stronger field strengths as solar activity intensifies.

ISSN 3084-8792

9 773084 879008

JOURNAL OF ECO ASTRONOMY

Sumanarathna, A. R., & Mayadunna, W. M. U. I. (2025). Multidisciplinary Benefits of the Near-Earth Interplanetary Coronal Mass Ejection Dataset (1996–2024) compiled by Richardson & Cane. *Journal of Eco Astronomy*, *01–01*(2), JEA 2025-15.

DOI: 10.63119/JEA15.2025